The Pennsylvania State University

The Graduate School

Materials Science and Engineering

FUNDAMENTAL STUDIES OF GLASS/POLYCARBONATE INTERFACE FOR COMPOSITE MATERIALS APPLICATION

A Thesis in

Materials Science and Engineering

by

Romesh J. Patel

Submitted in Partial Fulfillment
of the Requirements
for the Degree of

Master of Science

May 2008

The thesis of Romesh J. Patel was reviewed and approved* by the following:

Evangelos Manias
Associate Professor of Materials Science and Engineering
Thesis Advisor

Ronald Hedden
Assistant Professor of Materials Science and Engineering

Charles E. Bakis
Professor of Engineering Science and Mechanics

James P. Runt
Associate Head of Graduate Studies
Professor of Polymer Science

*Signatures are on file in the Graduate School

ABSTRACT

Glass fiber composites have tremendous success in industrial applications because they provide a light weight, high performance, polymer based alternative to other materials for certain uses. Glass fiber composites exploit the mechanical performance of the glass, paired with the light weight nature of the polymer. During industrial processing, glass fibers are easily incorporated into the polymer matrix using conventional mechanical processes such as extrusion or are incorporated as a mesh. As with any composites, the interface between the polymer and the glass play a vital role in determining the mechanical properties of the final material. Commercially, the glass surface is manipulated by using silane coupling agents that bond covalently to the surface. Although glass fibers are now widely used, there is little understanding about the interface between the glass fibers and most polymer matrices. Many scientists have attempted to study the interface by performing micromechanical tests between a single fiber and the polymer matrix. One such test is known as the single fiber pullout test. In this study, the pullout test is employed to study the interface between polycarbonate and glass fibers that have been treated with different silanes. Furthermore, the respective composites with 10 wt% glass fibers in polycarbonate are tested for their mechanical properties (the glass fibers used here were also treated with the same silanes as in the pullout tests). The results from the pullout tests show consistency with theoretical arguments, and correlate to the composites tests.

TABLE OF CONTENTS

LIST OF FIGURES

LIST OF TABLES

ACKNOWLEDGEMENTS

My sincerest thanks go to Bayer Material Science for providing funding and many of the materials for this project. I would also like to thank Dr. Evangelos Manias for giving me this opportunity to educate myself. His help, guidance, patience, and advice are greatly appreciated. I am also grateful to my other committee members, Dr. Ronald Hedden and Dr. Charles Bakis, for agreeing to be on my committee on a short notice, and for taking their time to evaluate this thesis and provide their much appreciated inputs.

It would also like to thank my colleagues, Rob Schaut and Bret Neese, for helping me at various stages of this project. I hope to return the favor someday.

My lab-mates, Theresa, Greg, Matt, Ngoh, Phon, George, and Jinguo have been very supportive in the project, and for that I would like to thank them.

Most importantly, I would like to thank my parents, Prafulaben and Jayantibhai, and my family; Archana, Prashant, Nisha, Harshal, Anuja, and Roger, for supporting and encouraging me in all my decisions, albeit some choices I made were doubtful. I cannot thank them enough. Finally, I dedicate this thesis to my parents and grand parents, Jaadaben and Maganbhai.

Chapter 1 Current Understanding of Micro Fiber/Polymer Interfaces and Composite Mechanical Properties

1.1 Introduction

Polycarbonate (PC) is a high performance polymer that has recently made great progress in industry as a commodity polymer. PC is considered a high performance polymer because of its superior mechanical properties, which provide new opportunities in structural applications. Its lightweight and transparent nature makes it an ideal candidate for optical applications from eyewear to window panels for skyscrapers and aircrafts. Many engineering applications now require polymers with improved mechanical properties, and although polymer blending and copolymerization are often employed, composite formation is by far the most favored method for improving mechanical performances of polymers. Reinforcing PC is also being widely practiced, resulting in mechanically robust but hazy materials.

In most polymer composite materials, glass fibers or carbon fibers are generally the reinforcements of choice[1-6]. Glass fibers get particular attention because they are cost effective and easily produced[4]. They are versatile in their uses in that, their mechanical, electrical, and chemical properties can be tailored by simply manipulating their composition[7].

During processing, the compounds are fed continuously to a furnace where they melt and fuse together to form molten glass, which is then drawn directly into fibers. The

fibers are then cooled and treated with organic coatings including reactive silane coupling agents, followed by more organic coatings that protect the fibers from environmental damage. The fibers can then be chopped or packed into spindles based on client requirements[7,8].

1.2 Conventional Interfacial Testing Methods

Many micromechanical tests have been devised to study the glass fiber-polymer interface, and almost all of them involve examining the interface between a single fiber and a polymer matrix. These tests include single fiber pullout tests[2,3,9,10], microdebond tests[1,4], fragmentation tests[11-13], and microindentation tests[14,15], schematically shown below in Figure 1.1.

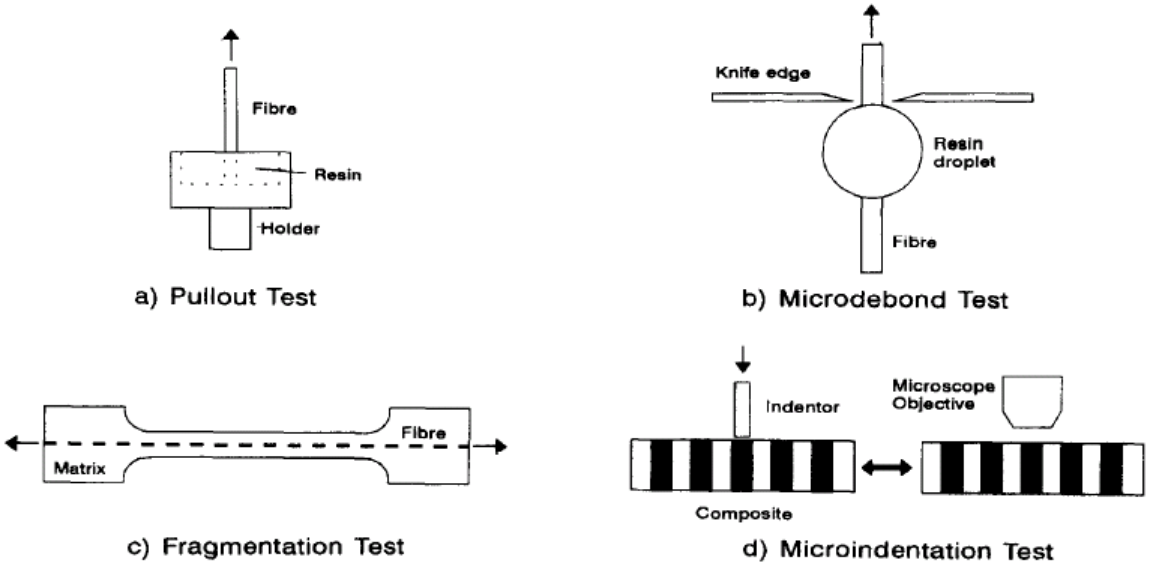

Figure 1.1. Micromechanical test techniques used to study the properties of the interface between fibers and polymer matrices (a) pullout test, (b) microdebond test, (c) fragmentation test, (d) microindentation test[14].

Both the pullout test and the microdebond test apply tension to a fiber that has a predetermined length embedded into the matrix. The microindentation test on the other hand uses compression. In all three tests, interfacial fracture is measured. In the fragmentation test, tension is applied to a polymer tensile bar with a long glass fiber aligned uniaxially to the load direction. The progressive fiber fracture is measured in this test. Micromechanical tests such as these have provided a direct method of studying the interface and its effects on mechanical properties[14].

In this study, the single fiber pullout test is utilized to obtain a quantitative understanding of the interfacial strength between PC and glass fibers. Self-assembled monolayers (SAMs) are synthesized on the fiber surface, using a variety of silanes, to determine and manipulate the interfacial adhesion between the modified fiber and the PC matrix. Further, composites are made using similarly modified fibers (as those employed in the pullout tests) and their mechanical properties are determined in order to study the correlation of the fiber-PC interfacial shear stress (τ_{IFFS}) and the Young's modulus of the composites.

1.3 Recent Progress in Interfacial Studies

Although the dependence of composite performance on the reinforcement-matrix interface is widely accepted[1-3], the exact stress transfer mechanism is highly ambiguous[14]. This is particularly true for polymer based composites, where a number of factors, such as polymer crystallinity, often play an important role. Micromechanical tests, including the single fiber pullout test, have been devised to study such interfaces and their impact on mechanical properties of composites. The single fiber pullout test is

perhaps the most interesting because it can be easily applied at different length scales from macroscopic materials such as rebar and concrete systems[16], down to the nanoscopic scale using carbon nanotubes and a polymer matrix[17-19].

The nanotube pullout test employs the same concepts that apply to the microscopic or macroscopic fiber tests. In an innovative experiment conducted by Barber et al[19], multi-walled carbon nanotubes (CNT) were attached to Atomic Force Microscopy (AFM) tips and were withdrawn from polyethylene-butene copolymer (PEB). Embedding of CNT into (PEB) was accomplished by melting the polymer and lowering the fiber-bearing tip into the matrix using the AFM. The polymer was cooled to 30 ^{O}C, and the tip was retracted from the sample to obtain a force-distance curve as the CNT was pulled out. A distinct peak in the force-distance curve was obtained, indicating the detachment of the embedded nanotube from PEB. AFM was later done on the sample to determine the embedded length. Figures 1.2 and 1.3 show a force versus time curve shown in the study, along with an AFM image of the exit hole and the corresponding cross-section used to get the embedded length. The time-axis shown in figure 1.2 indicates the time it takes to retract the tip from the sample. Given the retraction speed, the distance traveled by the tip in the z-direction can be calculated from the curve. The interfacial shear strength (τ_{IFSS}) was reported to be 47 MPa[19], calculated by: (Eqn 1.1)

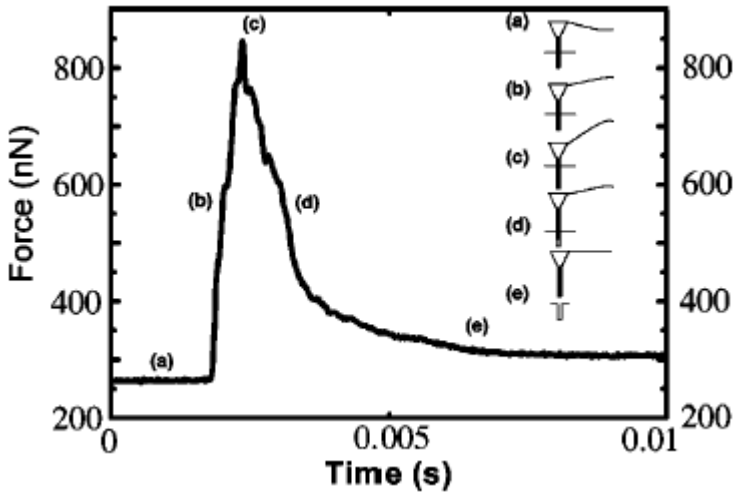

Figure 1.2 Force-time curve obtained during a CNT pullout test from PEB using an AFM. Designations (a) – (e) correspond to the schematic in the inset[19].

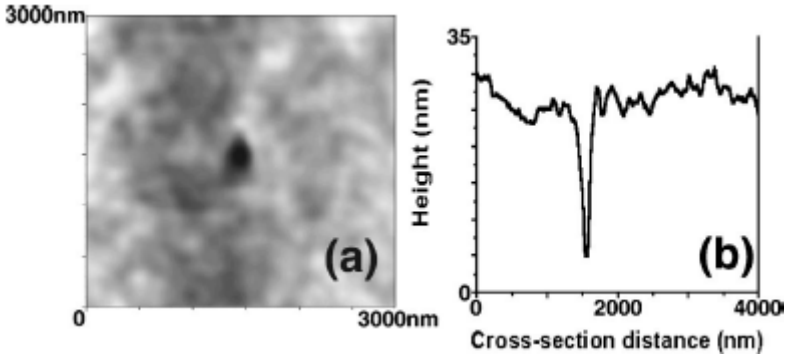

Figure 1.3 (a) AFM image of exit hole in PEB after the pullout test (b) Cross-section of the hole used to determine the embedded length[19].

$$\tau_{IFSS} = \frac{F_{\max}}{2\pi r_{NT} l_{emb}} \qquad \text{(Equation 1.1)}$$

where F_{max} is the maximum pullout force, l_{emb} is the embedded length, and r_{NT} is the nanotube radius. The τ_{IFSS} value reported for the CNT-PEB system is comparable to, or in some cases exceeds, those reported for glass fiber and carbon fiber – polymer systems. The drawback to CNT based composites (or in general nanocomposites) is that CNT surfaces are typically only modified to overcome agglomeration, and much less to

enhance adhesion with the matrix. The research discussed here does provide such providence.

Pullout tests can also be performed much easily when using thermosets, as shown by Piggott and Xiong[19]. In their experiment, the authors studied the debonding between commercially acquired glass fibers and a room-temperature-cured epoxy. The embedded length of the fiber could be precisely chosen because of the ease of using a liquid resin and precursor. Although they did not study surface modifications of any kind, the authors provided insight into the debonding mechanism. Other variables such as embedded length and curing time were observed as well. Although they determined that the debonding initiation force did not change with l_{emb}, they did notice its increase with epoxy curing time and temperature (from room temperature to 70 ^{O}C).

Feller and Grohens[4] used silane coupling agents to study their effect on a glass fiber and polypropylene-diene copolymer (PPD) system. The microdrop test was used in this instance, and the values τ_{IFSS} values reported ranged from 4-11 MPa. In contrast with most other studies, the authors found no agreement between the interfacial work of adhesion (W_{adh}) and τ_{IFSS}. The reasoning provided was that the adhesion between PPD and the coupling agent was not purely thermodynamic, but resulted from interdiffusion of the chains and covalent bonding. It should be noted that the coupling agents were not reacted with the glass fibers using conventional techniques. Instead, silanes were graft copolymerized with propylene and dienes, and coated onto the fibers, with the intention of cocrystallizing the fiber coating and the polymer matrix.

A similar system was examined by Mader et al[3], where pullout experiments were conducted on glass fibers embedded in a PP matrix. The variable in this experiment was

the PP matrix that was blended with a commercial modifier (maleic anhydride grafted PP), resulting in tripling of the polar component of the polymer's surface energy. Different film formers (protective coatings) were also applied to the fibers and the pullout experiments compared τ_{IFSS} between neat and blended PP. In all cases, the blended PP matrix resulted in an increase in τ_{IFF} by upto 73% compared to the neat PP matrix, showing a definitive correlation between high τ_{IFSS} and high fiber-matrix interfacial surface energies.

Although matrix and film former modifications can influence the interfacial adhesion, silanizing glass surfaces is the most popular method used in fundamental research. Glass surface chemistry has been studied extensively and the reaction between coupling agents and the hydroxyl groups on the glass surface are well understood.

Hoecker and Karger-Kocsis[1] examined the behavior of the interface between glass fibers and epoxy with a change in the surface treatment of the glass. Commercial fibers with different sizings along with unsized (bare) fibers were studied in this experiment using the microdebond test. The fiber differed in total surface energies ranging from 41 mJ m^{-2} to 52 mJ m^{-2} and τ_{IFSS} ranged from 42 MPa to 65 MPa, following the same trend as the surface energies. Unidirectionally oriented composite samples were also made of the same materials as the microdebond test, and tensile and torsion tests were conducted on the samples. A positive correlation was found between the macromechanical properties and τ_{IFSS}.

In a different study, Mader et al[2] conducted pullout tests on glass and carbon fibers that had been surface modified. A PP matrix was used and a linear correlation

between thermodynamic (interfacial) work of adhesion and τ_{IFSS} was found for both fiber types, with a few exceptions attributed to a 'chemical adhesion mechanism'[2].

Carbon fibers have comparatively better properties than glass fibers, however, due to their high cost; they are not as widely used as glass fibers. Nonetheless, their surface, much like the glass surface, can be modified to suit one's needs.

Pullout tests conducted by Ramanathan et al.[10] involved carbon fiber pullouts using PC as the matrix. In this study, the Energy Release Rate (ERR) was calculated and was found to increase proportionally with higher frictional force (friction between the carbon fiber and polymer)[10].

1.4 Outlook

Extensive literature review revealed that no micromechanical tests have been conducted on glass fiber-PC systems (there was one study devoted to understanding the pullout mechanism for carbon fiber-PC systems[10]). The brittle nature of the glass fibers imposes challenges during the pullout experiment, and the high melting temperature of PC limits the number of techniques that can be used to prepare single fiber pullout samples.

In this thesis, silane coupling agents are used to control interactions between the glass fiber and PC. The terminal groups of the silanes are chosen so as to incorporate four substantially different types of fiber-polymer interactions discussed in chapter 2. Silanization reactions were carried out in solution, and therefore monofunctional silanes were used in all cases. The Lifshitz-van der Waals and polar interactions are studied using silanes terminated with a methyl group and a trifluoro-methyl group. In addition,

surface energies of the unsilanized fibers are also taken into account. Hydrogen bonding interactions are examined using silanes that have an amine terminal group that should hydrogen bond with the oxygen atoms in the PC backbone (although these same amines may cause PC degradation). Finally, an ester terminated silane is used to facilitate a transesterification reaction with the PC backbone. Transesterification would occur between the alcoholic group on the silane and the carbonate on the PC backbone. In the reaction, the methoxy terminal group of the silane would attack the carboxyl group on PC, initiating the chain cleavage. A covalent bond would therefore be formed between the silane and PC. Figure 1.4 illustrates the two possible types of interactions. Micromechanical and macromechanical tests are conducted to determine the impact of interfacial adhesion on the mechanical properties.

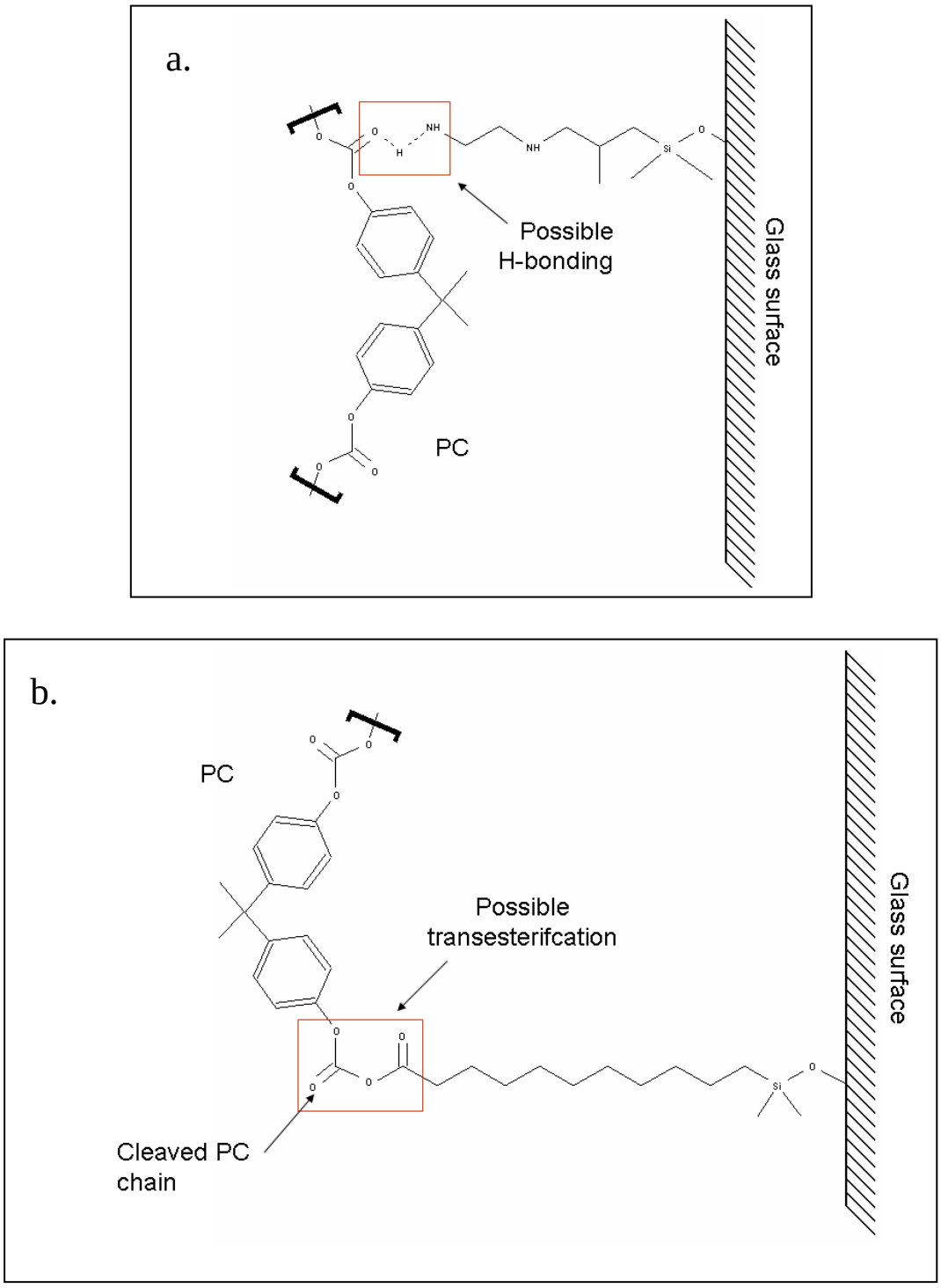

Figure 1.4 Illustration of anticipated a) H-bonding and b) covalent bonding via transesterification between PC and the two silanes used in the study.

Chapter 2 Study of Glass Fiber/PC Interface: A Theoretical Approach

2.1 Introduction

As indicated earlier, the mechanical performance of composites can be determined also by the strength and nature of the interface between the reinforcement and the matrix. In glass fiber/polymer composites, the interface facilitates stress transfer from the matrix to the fiber. The efficiency of this transfer is greatly dependent on the fiber-matrix interfacial strength. It is therefore apparent that the interfacial interactions between the fiber and matrix are important, and their control essentially determines the mechanical properties of the final composites.

2.1.1 Surface Energetics

To understand the pertinent surface interactions, it is important to understand surface energetics and their impact on the interfacial adhesion. The four distinct types of surface interactions considered in this study are,

- Lifshitz-van der Waals (LW) interactions,
- Lewis acid-base (AB) interactions,
- Hydrogen bonding,
- Covalent bonding.

LW interactions result from fluctuating dipole-dipole interactions between two given particles[20]. They are relatively weak and short-ranged since they decay rapidly with intermolecular distance. LW interactions are best described by the Lennard-Jones potential[21] function (Eqn 2.1), where the relation between interparticle distance and interaction energy is described as follows,

$$V(r) = 4\varepsilon\left[\left(\frac{\sigma}{r}\right)^{12} - \left(\frac{\sigma}{r}\right)^{6}\right] \qquad \text{(Equation 2.1)}$$

where V(r) is the potential, ε is the pair attraction potential well depth, σ is the atomic diameter, and r is the distance between the centers of the two atoms[21]. Lewis acid-base interactions; where present, are typically stronger than LW interactions, and decay slower with increasing molecular distance (r^{-4} instead of r^{-6})[21]. LW and AB interactions can be calculated using the surface energies of the interacting components, where the surface energy of one component is described by Equation 2.2.

$$\gamma_s = \gamma_s^{LW} + \gamma_s^{AB} \quad \text{where} \quad \gamma_s^{AB} = 2\sqrt{\gamma_s^{+}\gamma_s^{-}} \qquad \text{(Equation 2.2)}$$

Where γ_s is the total solid surface energy, γ_s^{LW} and γ_s^{AB} are the apolar and polar portions of solids surface energy, respectively, and γ_s^{+} and γ_s^{-} are the acid and base contributions to the polar surface energy, respectively. Van Oss[20] suggested that because these interactions are polar in nature (electron acceptor-electron donor), they are asymmetrical and this asymmetry needs to be accounted for by breaking γ^{AB} into two portions as shown in Equation 2.2. To obtain γ_s^{LW}, γ_s^{+}, γ_s^{-} values, contact angle measurements can be performed using three liquids with known surface energies, of which one should be apolar ($\gamma_l^{+} = \gamma_l^{-} = 0$), and two should be polar[20]. When a drop of a liquid is placed on a

flat surface, its ability to wet the surface is determined by the surface energy of the liquid, the surface energy of the solid, and the interfacial energy between the solid and liquid. The degree of spreading is quantified by the contact angle that results when a drop adopts the equilibrium quasi-spherical shape on the surface. Interfacial LW and AB interactions between the solid and liquid (γ_{sl}), solid and vapor (γ_{sv}), and liquid and vapor (γ_{lv}), acting upon the drop, define the contact angle, as shown in Figure 2.1. These interactions between any two surfaces can be measured using Equation 2.3, where v, s, and l are used interchangeably.

$$\gamma_{sl} = \sqrt{\gamma_s^{LW}\gamma_l^{LW}} + \sqrt{\gamma_s^{+}\gamma_l^{-}} + \sqrt{\gamma_s^{-}\gamma_l^{+}} \qquad \text{(Equation 2.3)}$$

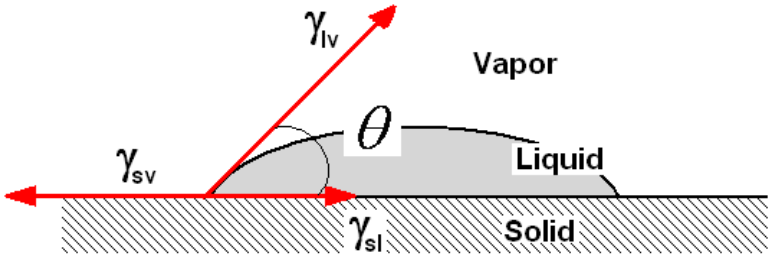

Figure 2.1 Force equilibrium for a sessile drop, showing contact angle between the solid and liquid phase[1].

Using experimental contact angles, with two polar liquids and one apolar liquid with known γ_l^{LW}, γ_l^{+}, and γ_l^{-} values, γ_s^{LW}, γ_s^{+}, and γ_s^{-} can be determined employing the Van Oss formalization (Eqn 2.4). γ_l is the total surface energy of the liquid.

$$(1+\cos\theta)\gamma_l = 2(\sqrt{\gamma_s^{LW}\gamma_l^{LW}} + \sqrt{\gamma_s^{+}\gamma_l^{-}} + \sqrt{\gamma_s^{-}\gamma_l^{+}}) \qquad \text{(Equation 2.4)}$$

The interfacial tension between two bodies, also known as work of adhesion, can also be easily calculated using,

$$(1+\cos\theta)\gamma_l = W_{adh} \qquad \text{(Equation 2.5)}$$

An alternate theory, known as the Owen-Wendt approach, is simpler than the Van Oss approach because it does not break γ^{AB} into two terms, rather define it as a whole, polar portion of surface energy, γ^p. Therefore, all the equations presented above simplify to the following[1,4,23,24]. γ^{LW} is defined as γ^d, for dispersive surface energy.

$$(1+\cos\theta)\gamma_l = W_{adh} = 2(\sqrt{\gamma_s^d \gamma_l^d} + \sqrt{\gamma_s^p \gamma_l^p}) \qquad \text{(Equation 2.6)}$$

Hydrogen bonding is also a dipole-dipole type interaction where two electronegative atoms such as nitrogen and oxygen "share" a hydrogen atom. It is stronger than polar interactions[25], however, it is substantially short ranged.

Finally, covalent bonds between two particles can be considered the strongest types of interactions, and such bonds are highly desirable in composites between the various components (e.g. between filler and matrix) when mechanical performance is essential[25].

In glass fiber-polymer composites, the surface of the glass is easily manipulated compared to that of the polymer. Therefore, most interfacial interventions can be done on the glass surface. The simplest way of doing this is by using silane coupling agents.

2.1.2 Silane Chemistry

Silane coupling agents can be easily applied to a glass surface because the hydroxyl groups that reside on the glass react readily with silane coupling agents[25-27]. Silane molecules are made of three distinct parts, namely the head, spacer, and terminal groups. The head group is responsible for bonding covalently with the glass surface's

hydroxyl groups. The spacer group creates distance between the glass surface and the terminal group, and can facilitate SAM packing when long enough. The terminal group essentially alters the glass' characteristics (reactivity, surface energy, etc) assuming a good coverage so that only the terminal groups are exposed. Figure 2.2 illustrates a typical silane molecule with the three groups discussed.

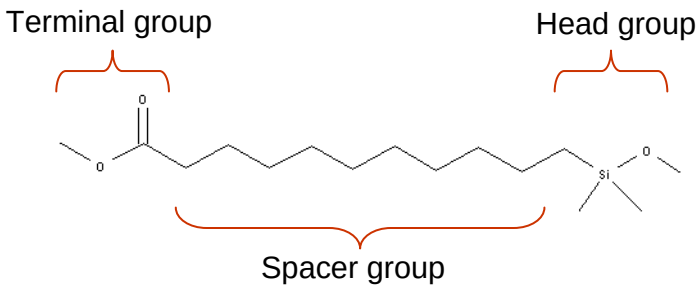

Figure 2.2 Example of a silane molecule showing its different structural components. The head group attaches to the glass surface via covalent bond. The terminal group gives the glass surface its functionality.

The head group consists of a silicon atom that is bonded to the spacer group and up to three functional groups. In Figure 2.2, the head group has one functional group, the methoxy group, attached to it. Multifunctional groups can also be used to increase the reactivity of the head group with the surface; however, it also permits some side reactions. In the case of monofunctional silanes, the only possible reaction is between one hydroxyl group on the glass and the silicon atom on the silane. In the case of multifunctional silanes, the silicon atom may attach to multiple hydroxyls on the glass, or, react with other silane molecules, thereby polymerizing on the glass surface or in solution. Figure 2.3 gives a detailed description of all such possible reactions.

As it is seen in Figure 2.3, creation of a well defined SAM is not always guaranteed when using multifunctional silanes.

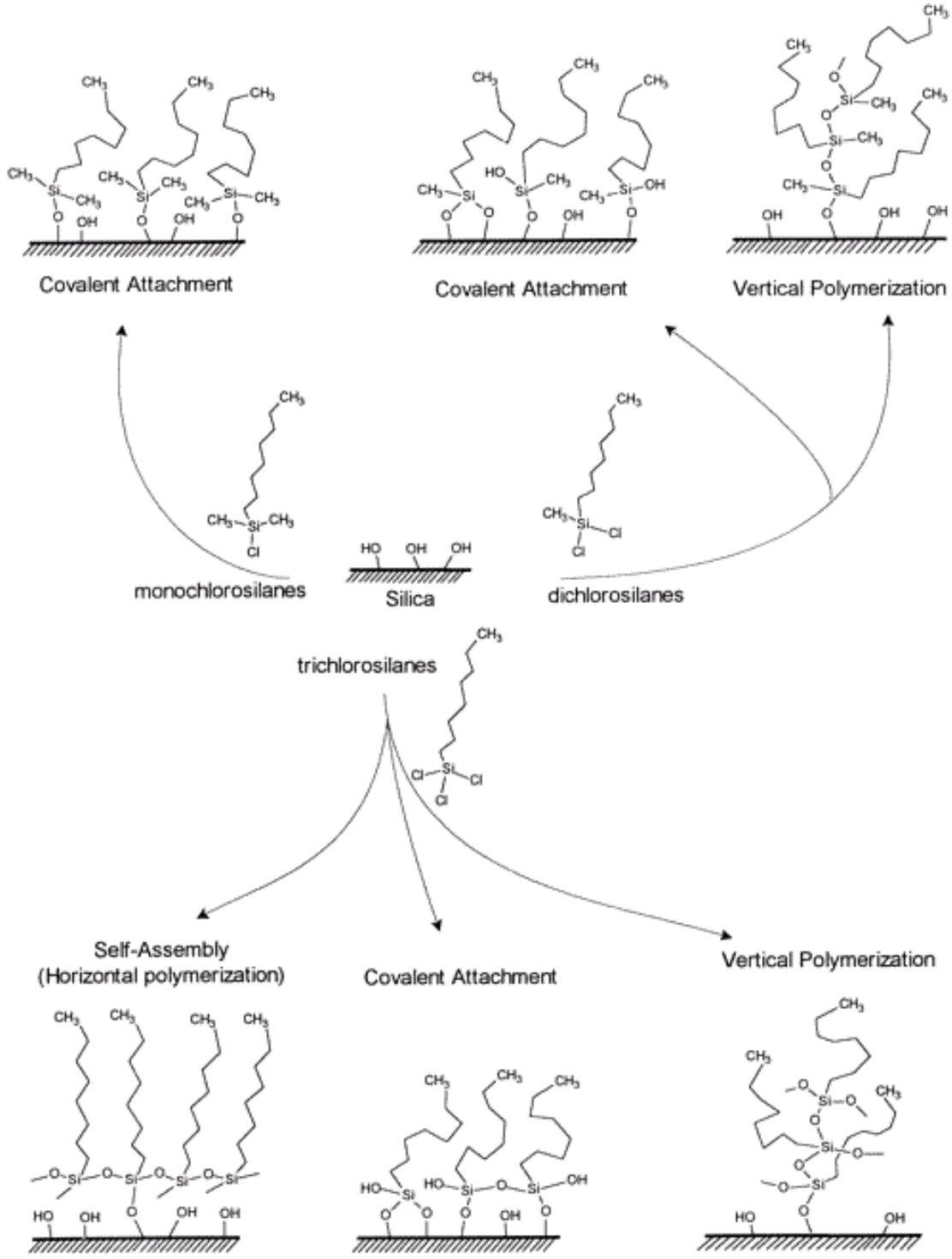

Figure 2.3 Possible reactions between mono or multi functional silanes and glass surface. Side reactions possible with multi functional silanes include reactions with other silane molecules[26].

The reactivity of the silane to the glass can be further modified by the type of functional group attached to the silicon atom. Conventionally, three functional groups are used; ethoxy- ($-OCH_2CH_3$), methoxy- ($-OCH_3$), and chlorine (-Cl), with ethoxy silanes being the least reactive and chlorosilanes being the most reactive[26].

The mechanism of the silanization reaction can be described as follows. Electrons from the oxygen atom of the hydroxyl group on the glass surface attack the silicon atom of the silane molecule. The positive charge created on the oxygen and silicon atom forces the expulsion of the hydrogen atom and the functional group respectively. The expelled hydrogen atom and the expelled fragment of the functional group form to an acid in the solution. In the case of methoxy-, and ethoxy- silanes, these functional groups are first hydrolyzed before reacting with the glass[25,26]. It is therefore easy to comprehend that the interactions between the glass and matrix can be easily influenced by simply incorporating the silane onto the glass surface, and selecting the terminal surfactant group appropriately.

2.2 Experimental

Materials

E-glass fibers for the pullout test ranging in diameter from 45 μm to 90 μm were drawn using the glass melting furnace at the Materials Research Institute. The glass was melted at 1050 ^{O}C and was allowed to flow out from the hole at the bottom of the furnace, assisted only by gravity. This allowed the glass to flow slowly and therefore resulted in fibers with relatively thick diameters, suitable for pullout tests. Pyrex fibers were obtained by melting a pyrex rod and stretching it while molten. The silanes used in

this experiment were N-Butyldimethyl chlorosilane (BDMCS), Tridecafluoro-1,1,2,2, tetrahydrooctyldimethyl chlorosilane (TFCS), Octyldimethyl methoxysilane (ODMS), N-(2-aminoethyl) 3-aminoisobuytldimethyl methoxysilane (NHDMS), and 10-(carbomethoxy) decyldimethyl methoxysilane (CDDMS). Structure figures of these silanes are shown in Figure 2.4, and the names in parentheses are the names assigned to the fibers functionalized with these silanes. Polycarbonate powder (Makrolon 5308) used for the pullout test was obtained from Bayer.

BDMCS (CH_3 fiber)	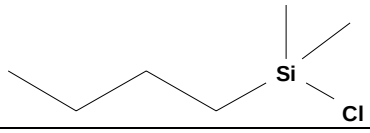
TFCS (CF_3 fiber)	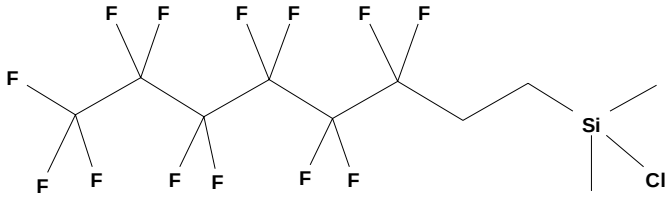
ODMS	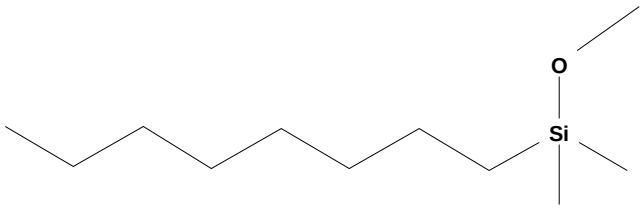
NHDMS (NH_2 fiber)	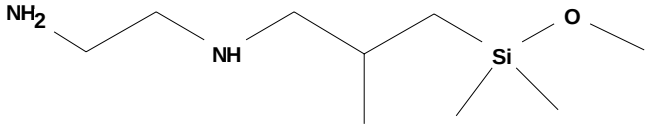
CDDMS (OCH_3 fiber)	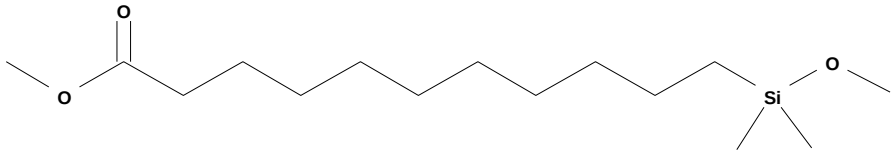

Figure 2.4 Structures of silanes used to form monolayers on the glass surface. Names in parenthesis are designated to the fibers functionalized with the silane.

BDMCS and TFCS gave the glass surface alternate surface tensions, thereby allowing the study of surface tension effects on interfacial adhesion and τ_{IFSS}. NHDMS would supposedly give the fiber hydrogen bonding (with PC) capability, and CDDMS would possibly take part in transesterication with the PC chain. ODMS was used as a 'filler' silane for NHDMS and CDDMS, in order to prevent complete coverage of the glass with the latter two silanes.

Silanizing Glass Fibers

The glass fibers were chopped into ~5 cm fibers and submerged in a solution containing the silane. Different silanes required different coating procedures. 1.0 ml of BDMCS was added to 400 ml of hexane, and the solution was stirred until it turned clear. The solution was mixed for another five minutes before the fibers were added to it. The glass fibers were stirred occasionally in the solution for 2 hours, after which they were removed and sonicated in methanol for ~10 minutes. Sonication is done to remove any physisorbed silanes from the glass. The glass fibers were removed from the methanol, spread on aluminum foil, and dried in a vacuum oven at 100 ^{O}C for 2 hours.

The same procedure is used to silanize the glass fibers with TFCS. 1.5 ml of TFCS was added to 50 ml of hexane. Unlike BDMCS however, the fibers were left in the silane solution for 6 hours instead of 2 hours.

In the case of NHDMS, 25%/75% ODMS/NHDMS mixed monolayers were grown on the glass fibers instead of complete coverage with the individual silanes in order to limit the amount amine groups per surface area. The preparation conditions for these are as follows. 0.3 ml of ODMS was added to 72 ml of toluene. In a separate

beaker, 0.1 ml of NHDMS was added to 24 ml of toluene. Both solutions were mixed until clear, and further stirred for five more minutes. The two solutions were then mixed together and mixed for 15-20 minutes before dipping the fibers into the solution. The fibers were left in the solution overnight while continuously being stirred. Washing in methanol and drying followed as before. ODMS was used as a diluent silane because its head group and spacer group are similar to those of NHDMS.

The same procedure is used for the CDDMS samples and here too ODMS was used as the diluent silane for the same reason as with NHDMS. Complete coverage with NHDMS and CDDMS is not desirable, since this would lead to exceptional adhesion, which would prevent interfacial debonding, and consequently, the pullout of the fiber.

Surface Energy Determination

Glass slides were treated in the same manner as the fibers in order to produce monolayers that were used for surface energy determination. Surface energies were derived using the contact angle method with a home-built contact angle set-up. The liquids used were millipore water and hexane.

Pullout Sample Preparation

For the pullout samples, it was important to embed the fiber in the matrix such that the matrix was homogenously distributed around the fiber. Therefore, PC was melted at 300 ^{O}C around a certain length of the fiber. The fiber had a free end to which piece of paper was attached with a drop of commercially available epoxy (as shown in Figure 2.6). Figure 2.5 is an illustration of the mold designed to make these samples.

An optical microscope was used to image the sample before and after the pullout to ensure a successful pullout occurred. This also helped confirm the embedment length obtained, an information that can also be derived a posteriori from the force-distance curve.

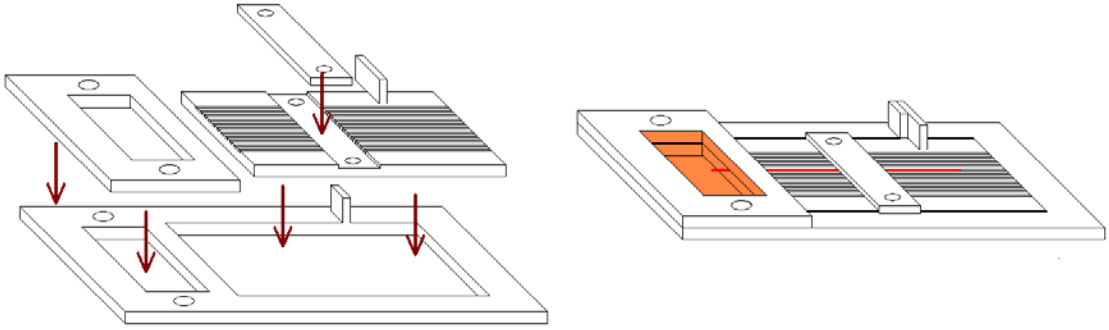

Figure 2.5 Mold designed to make pullout samples. Grooves ensure fiber is aligned perpendicularly to the polycarbonate block. Mold is made of aluminum.

Pullout Test

After attaching the free end of the fiber in the pullout samples to a piece of paper with an epoxy, the samples were vertically mounted on the tensile tester. The epoxy and paper were held by the grips on the cross-head, and because the fiber diameter was thick enough, it could sustain the weight of the epoxy and still remain vertical. A strain rate of 0.06 mm/min was used for this test. The interfacial shear stress (τ_{ifss}) was calculated using Equation 2.7.

$$\tau_{IFSS} = \frac{F_{\max}}{\pi D_f l_{emb}} \qquad \text{(Equation 2.7)}$$

Where the force, F_{max}, and the embedment length, l_{emb}, can be obtained from the force distance curve. The fiber diameter, D_f, was determined using an optical microscope. The figure below illustrates the sample dimensions and experimental set-up.

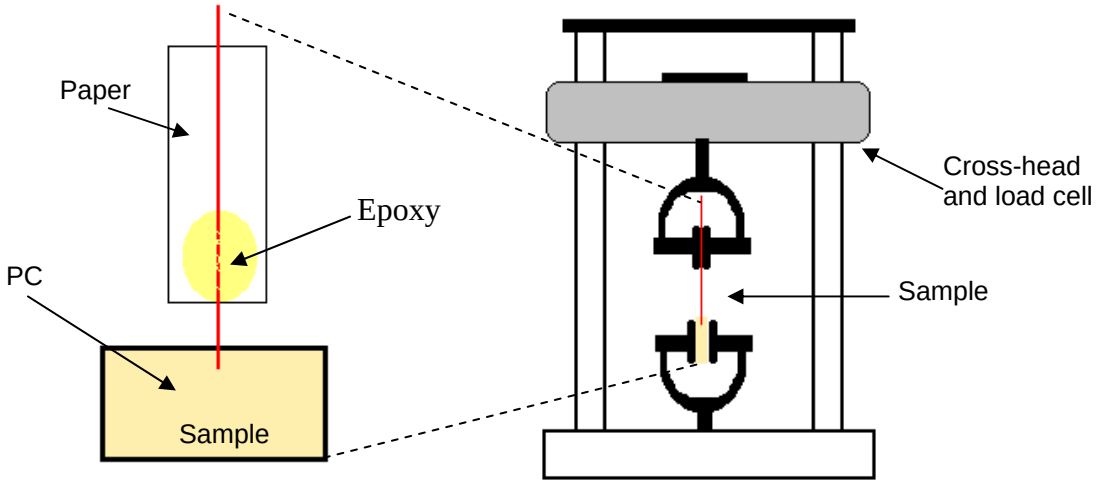

Figure 2.6 Schematic of single fiber pullout sample and pullout apparatus.

2.3 Results and Discussion

2..3.1 Fiber Surface Free Energy

The contact angle experiment provided the trend in hydrophobicity of the differently silanized glass slides. Since it is difficult to perform the contact angle experiment on the fibers, glass slides were used. The glass slides underwent the same silanizing treatments as the fibers. The obtained contact angles are shown in Figure 2.7. As expected the glass surface with the fluorine terminated silane (CF_3) was most hydrophobic, followed by the methyl terminated silane (CH_3), whereas the bare surface proved to be the most hydrophilic. These contact angles, given in Figure 2.7, agree reasonably well with literature (Table 2.1), therefore good monolayer coverage is assumed. Using contact angles, the surface energy of any solid can be measured easily using Equation 2.8. (same as Eqn 2.6),

$$\gamma_l(1+\cos\theta) = 2\sqrt{\gamma_s^d \gamma_l^d} + 2\sqrt{\gamma_s^p \gamma_l^p} \qquad \text{(Equation 2.8)}$$

where γ_l is the total surface energy of water, γ_l^d and γ_l^p are the apolar and polar surface tension components of water, and γ_s^d and γ_s^p are the apolar and polar surface tension components of the glass; θ is the contact angle formed by the water droplet on the glass slide. Typically, γ_l, γ_l^d and γ_l^p are known for two test liquids, one of which is apolar. After obtaining q for both liquids on the same glass surface, one can obtain γ_s^d and γ_s^p. The apolar test liquid has to have a relatively high surface energy. Due to this constraint, methylene iodide is commonly used since it is apolar and has a surface energy of 50.8 mJ m^{-2}. However, it is sensitive to light and therefore contact angle measurements using methylene iodide are done in the dark using an infra-red camera. Since the current experimental setup is not well suited for such tests, surface energy terms from literature are used instead. Therefore, literature based surface tension values are used to calculate W_{adh} (Eqn 2.9). This is justifiable since the contact angle measurements agree well with literature based values for water (Figure 2.7). Also, contact angle measurements could only be done using pyrex glass and not E-glass because a flat surface for measurements was not available for the E-glass. Table 2.1 shows the surface energy terms for the different fibers as well as for PC. The corresponding work of adhesion is calculated using the following equation.

$$W_{adh}^{PC} = 2\sqrt{\gamma_s^d \gamma_l^d} + 2\sqrt{\gamma_s^p \gamma_l^p} \qquad \text{(Equation 2.9)}$$

Table 2.1 Literature based contact angles and surface tension for the different silanes used in this reaction. Theoretical work of adhesion between silane and PC also given. Contact angle and surface energy values were obtained from [29,30].

Surface Energies and Work of adhesion (mJ / m^2)					
Material	θ	γ_s^d	γ_s^p	γ_s	W_{adh}^{PC}
CF_3 silane	107^O	11.45	1.77	13.22	42.40
CH_3 silane	100^O	24.65	0.79	25.44	56.80
Pyrex	9.8^O	37.68	21.84	59.52	88.44
NH_2 fiber	48^O	47.20	0.10	47.30	69.91
E-glass fiber		43.18	29.46	72.64	96.84
Polycarbonate		27.70	6.50	34.20	

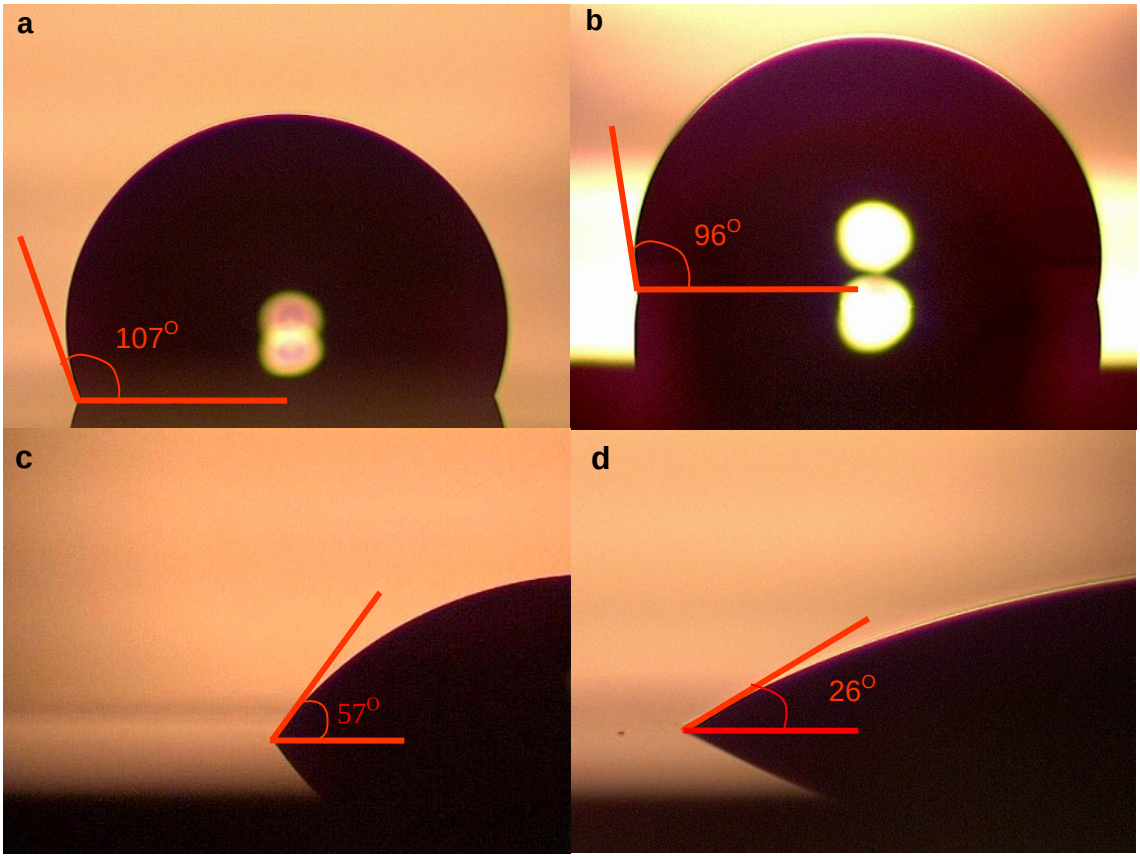

Figure 2.7 Contact angles formed by 5 µl water droplets on silanized glass slides. The surfaces are a) TFCS silanized, b) BDMCS silanized, c) NHDMS silanized, d) glass surface.

2.3.2 Pullout Test Results

Force-distance curves obtained during the pullout test provides vital information used to calculate the interfacial shear stress (Equation 2.7). A sample of the force distance curve is given in Figure 2.8.

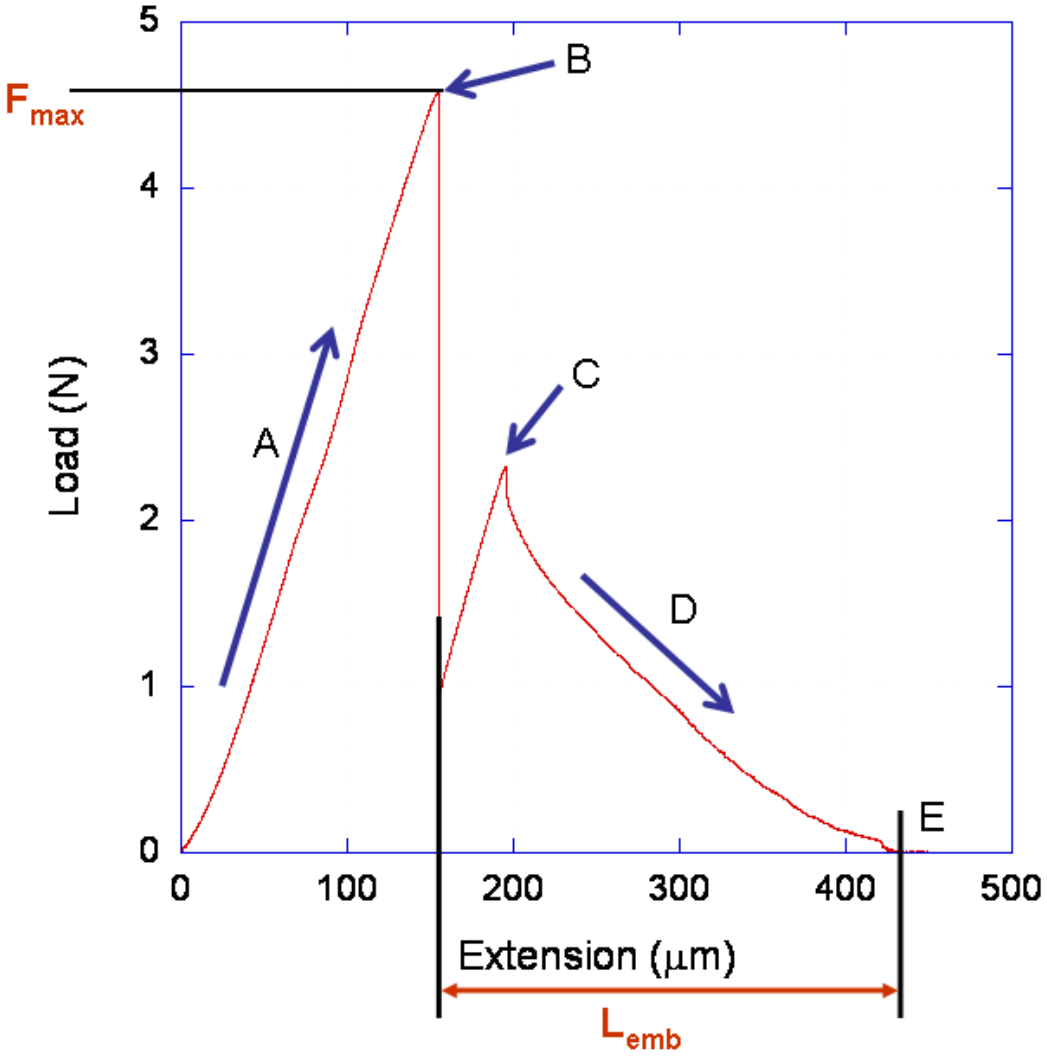

Figure 2.8 Example of a force-distance curve obtained during pullout experiment. (A) Sample experiencing tension before debonding, (B) Fiber debonding occurs, indicated by the sudden drop in force, (C) Maximum frictional force encountered during pullout, (D) Fiber sliding out from the matrix, (E) Fiber exits the PC.

Beginning at point A, the specimen experiences an increase in force as it is stretched. The slope of A is believed to represent elastic deformation leading to the interfacial break. Since glass fibers have a much greater modulus, this deformation is shared by the interface and the polymer. Deformation in the polymer can be seen in Figure 2.12, shown by the striations around the exit hole. Table 2.2 summarizes some of the properties of the materials, and the following figure illustrates the stress-strain curves of the different materials. It should be noted that the values given in Table 2.2 are from literature, whereas the stress-strain curves in Figure 2.9 are obtained experimentally.

Table 2.2 Some mechanical properties of E-glass[7] and PC[31]

	Tensile strength @ 23°C (MPa)	Modulus (GPa)	Elongation @ break (%)
E-glass	3100 - 3800	76 - 78	4.5 - 4.9
PC	72.4	2.2	100

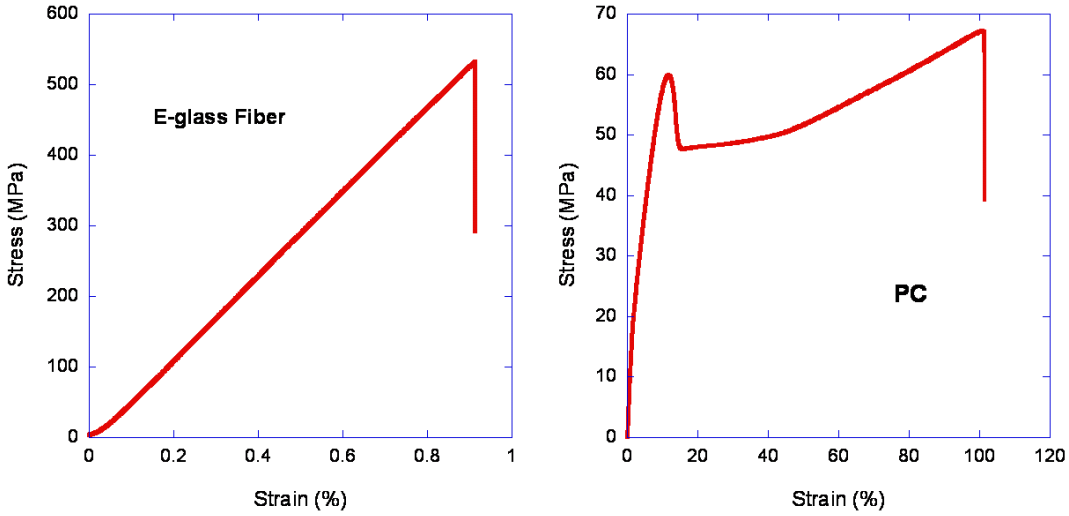

Figure 2.9 Typical stress-strain behavior for glass fibers and polycarbonate. Disparity in the scales indicates a superior Young's modulus for E-glass compared to PC. Single glass fiber (D = 60 μm) and PC tensile bar used to obtain curves.

At point B, the interfacial debonding fracture occurs, which is followed by a sharp drop in force. This fracture could indicate two possibilities, depending on the magnitude

interfacial adhesion between the fiber and matrix: if the adhesion is very strong, the fracture is most likely to be within the polymer; as a result, the polymer adjacent to the fiber will still be attached to the fiber after the pullout test. On the other hand, a weaker interface would result in an interfacial fracture, where the fiber cleanly detaches from the polymer. The latter case applied in all cases in this study, because of the observation of the pulled-out fibers (Figure 2.11).

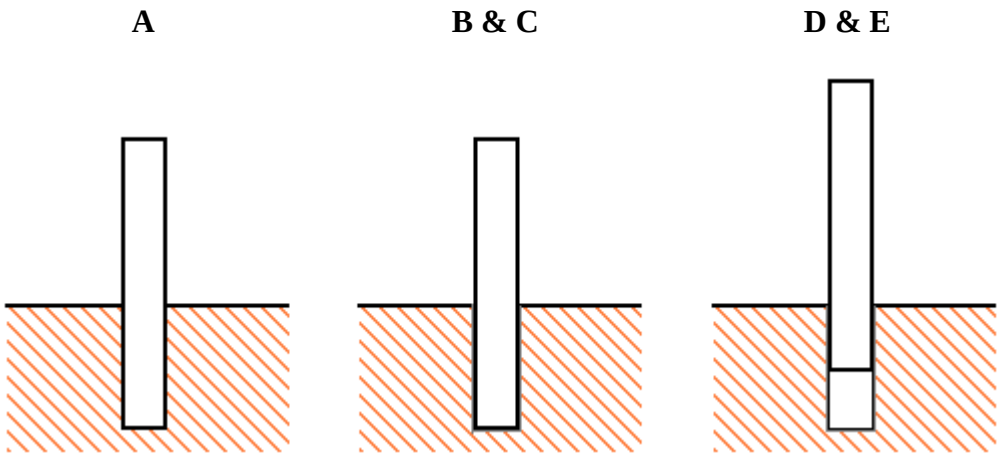

Figure 2.10 Schematic of sample during pullout test. A-E correspond to points A-E in Figure 2.8

The fiber continues to slide out of the PC matrix, shown as D, until it completely exits the sample (E). The pullout is shown schematically in Figure 2.10.

Two critical values, the maximum force (F_{max}), and the embedded length (L_{emb}), can be obtained from the force-distance curve shown in Figure 2.8. Figure 2.11 shows optical micrographs of one sample before and after the pullout test. Such images were used to verify the embedded length.

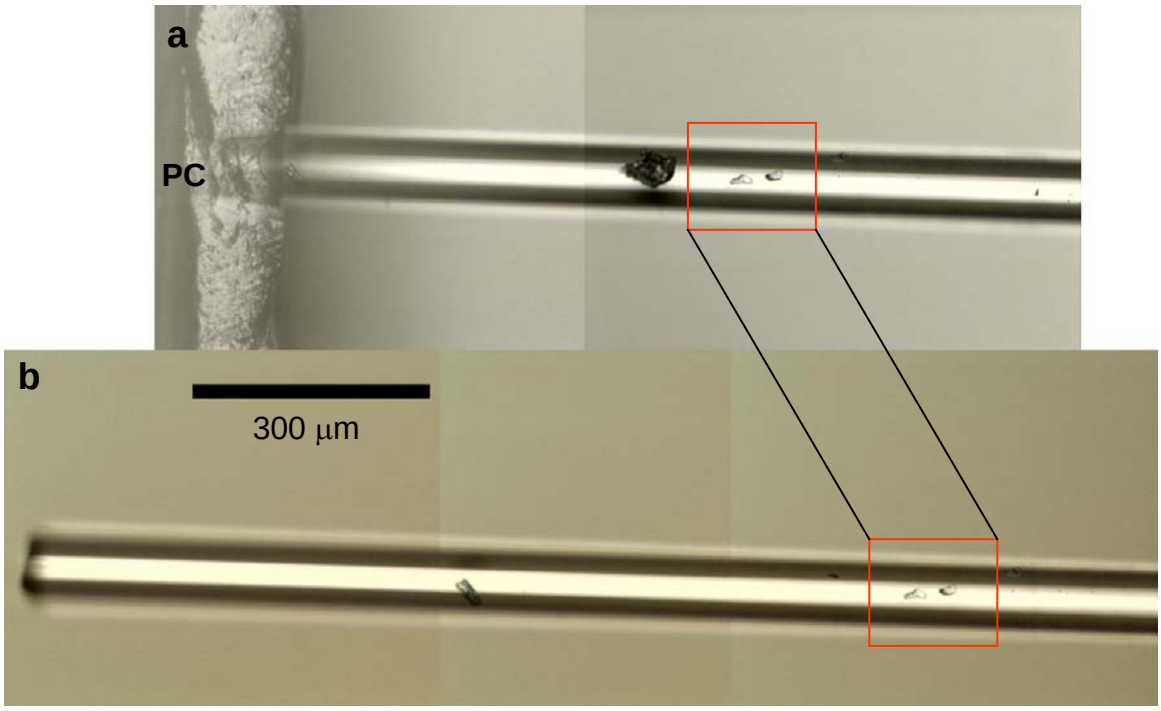

Figure 2.11 Optical images showing a fiber before and after pullout. The markings in the red box were used as indicators. (a) before pullout, (b) after pullout.

Table 2.3 summarizes the results obtained from the pullout tests. Figure 2.12 shows images of PC holes obtained after the pullout, and it is observed that the PC deformed slightly during pullout, indicated by the striations around the exit hole. This indicates that the total energy required to debond the interface also includes the energy required to deform PC, and the first portion of the pullout curve ('A' in Figure 2.8) signifies this deformation.

Table 2.3 Experimental data for glass fiber pullout. τ_{IFSS} is calculated using Equation 2.7.

Fiber type	pyrex	CH_3 -fiber	CF_3-fiber	E-glass	NH_2 fiber
lemb (m) $x10^{-5}$	3.7	25.4	45.9	20.4	44.7
diameter (m) $x10^{-5}$	13.8	10.8	8.3	7.6	4.9
Force (N)	0.8	3.8	4.2	3.1	2.7
Interfacial Area (m^2) $x10^{-7}$	1.6	8.7	1.2	4.9	6.9
τ_{IFSS} (MPa)	**48.1**	**43.4**	**34.8**	**62.5**	**40.1**

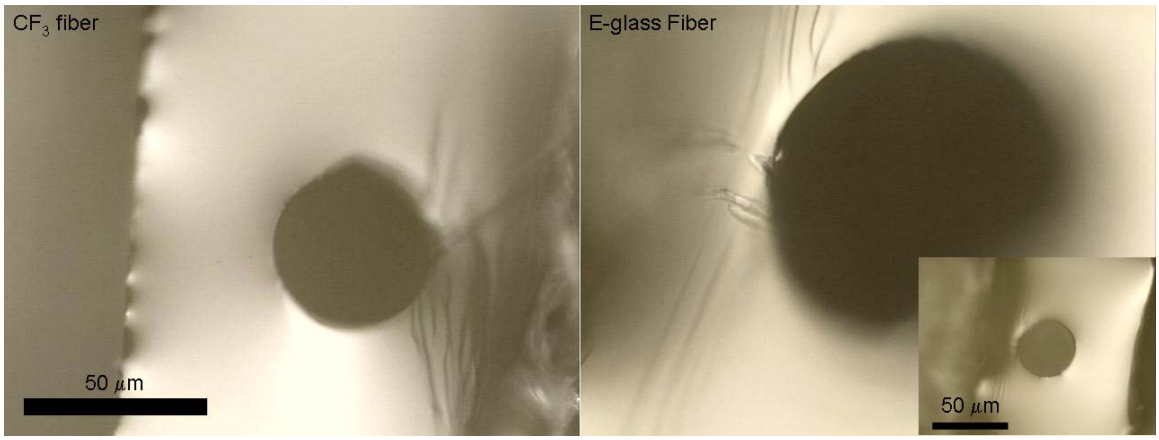

Figure 2.12 Exit holes in PC viewed after pullout test. Striations around the hole indicate PC deformation. Inset in E-glass fiber picture shows a zoomed out image of the same hole

The trend noticed in the τ_{IFSS} values is as expected for the first 4 samples. These samples interact with PC via dispersive-polar interactions only, and therefore Equation 2.9 could be applied to determine the work of adhesion for these samples. In Figure 2.13, the correlation between τ_{IFSS} and W_{adh} is illustrated.

The one exception in Table 2.3 is the NH_2 fiber, which was expected to have a much higher value because it is most likely to hydrogen bond with the PC. However, since only 25% of the surface is assumed to be grafted with NHDMS, it is possible that the portion of fiber embedded in PC was covered mostly with ODMS silanes (uneven coverage). The error bar for the NH_2 fiber in Figure 2.13 represents the error associated with having uneven concentration of the two silanes (ODMS and NHDMS) on the fiber. Table 2.4 provides an overview of typical strengths of covalent bonds and van der Waals interactions. It should be noted here that the hydrogen bond strength is comparable to the polar bond strength.

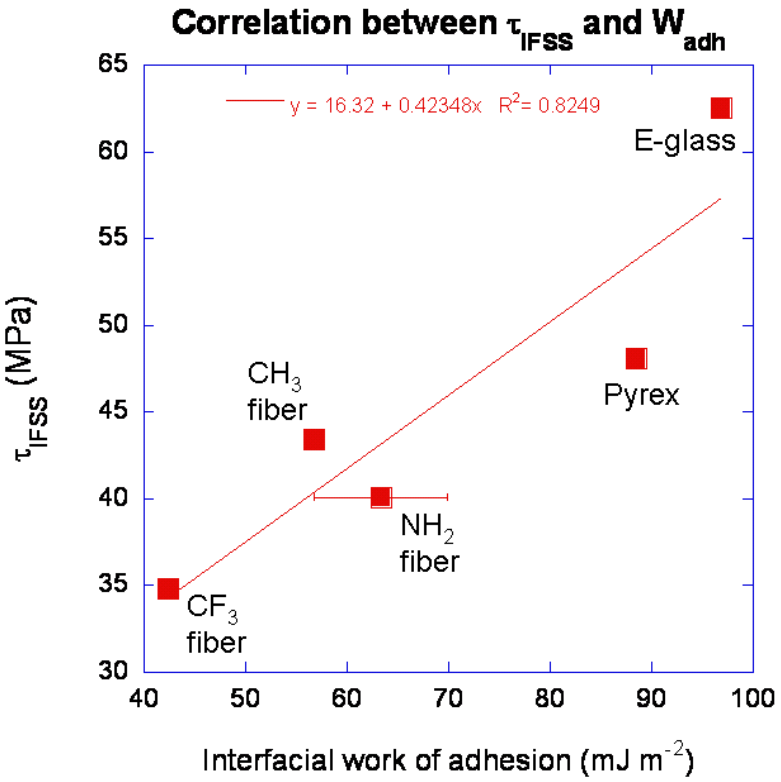

Figure 2.13 Correlation between the measured interfacial shear stress and calculated work of adhesion. The correlation shows that the interfacial shear stress increases somewhat linearly with the work of adhesion.

With the OCH_3 fibers, τ_{IFSS} values could not be obtained because the samples tested failed to pullout. In one instance, the fiber broke within the epoxy, debonded, and pulled out of the epoxy without any damage to the fiber-PC interface. Such behavior is not entirely unexpected because CDDMS should experience trans-esterification with the PC chain. During another attempt, the pullout failed to occur even at a high load of 4.6 N. Instead, the fiber broke resembling a tensile test. This implies that the CDDMS silane covalent bonds with the PC chain, resulting in a strong interface. Figure 2.14 shows the instance described above where the glass fiber pullout out of the epoxy.

Table 2.4 Typical bond energies associated with different kinds of bonds[25].

Type of interaction	Energy (kJ mol^{-1})
Ionic	
Na^+Cl^-	503
$Al^{3+}O^{2-}$	4290
$Ti^{4+}O^{2-}$	5340
Covalent	
C–C	368
C–O	377
Si–O	368
C–N	291
Hydrogen bond	
–OH···O=C– (Acetic acid)	30 ± 2
–OH···OH (Methanol)	32 ± 6
–OH···N (Phenol-trimethylamine)	35 ± 2
F^-···HF (Acetic acid)	163 ± 4
F^-···HOH (Acetic acid)	96 ± 4
Lewis acid–base	
$BF_3 + C_2H_5OC_2H_5$	64
$C_6H_5OH + NH_3$	33
$SO_2 + N(C_2H_5)_3$	43
$SO_2 + C_6H_6$	4.2
van der Waals forces	
Dipole–dipole	≥2
Dipole–induced dipole	0.05
Dispersion	≥2

Figure 2.14 OCH_3 fiber pullout from the epoxy grip. Fiber in PC remained intact. (a) before debonding from the epoxy, and (b) after debonding.

Another phenomenon noticed in the force-distance curves that is not discussed in literature is the slip-stick observed after the initial debonding. This can be observed in the noisy region of the curves (Figure 2.15). It is noticed that pullout curves for the unsilanized fibers produced no such behavior, while the silanized fibers did have a significant number of slip-stick events. This may be a result of the difference in the static and kinetic coefficients of the different fibers due to silanizing.

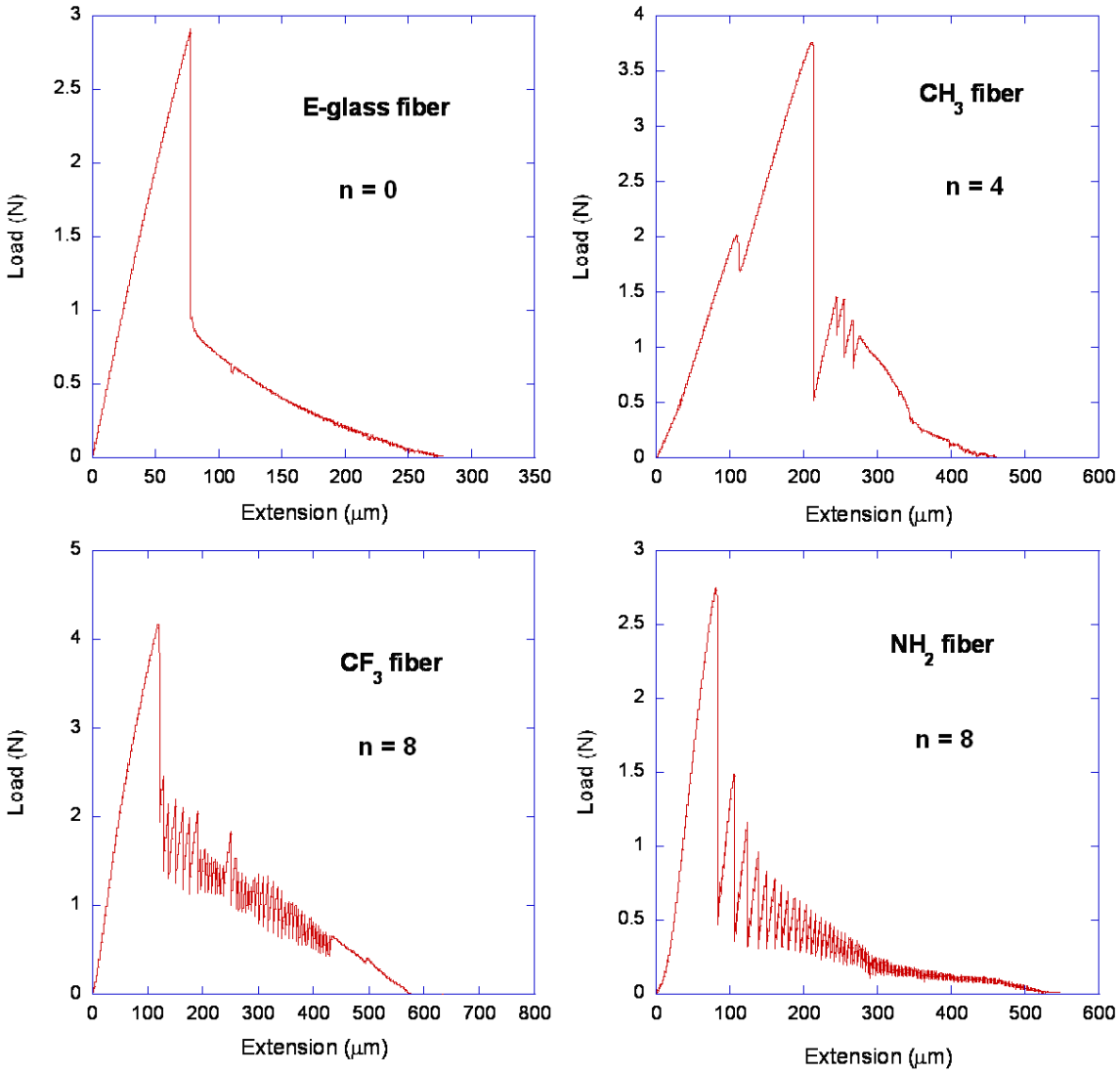

Figure 2.15 Force-distance curves for different fibers. Number and magnitude of stick-slip events.

2.4 Summary

Using the pullout test using silanized E-glass fibers and a polycarbonate matrix, it was proven that the τ_{IFSS} increased linearly with the W_{adh} resulting from the change in surface energy of the E-glass fibers. The pullout result for the NH_2 fiber was consistent based on surface energy calculations; however, it was expected to give a higher τ_{IFSS} value due to hydrogen bonding. As for the OCH_3 fibers, pullout experiments indicate towards stronger surface interaction, just as predicted. Finally, 'noisy' regions on the pullout curves after the debonding hint towards a difference in the static and kinetic coefficients of friction for the different fibers, with the unsilanized fibers having minimum difference, and the silanized fibers having the most.

Chapter 3 Role of Surface Interactions on Mechanical Properties of Fiber/PC Composites

3.1 Introduction

Glass fiber-polymer composites have tremendous success because they are light-weight, high-performance construction materials that are cost-effective and easily processed. Glass fibers are easily included in thermoplastics as well as thermosets. Because the fiber diameter is in the range of tens of microns, dispersion is not as problematic as with nanometer scaled reinforcements. This is because the intermolecular forces that are responsible for agglomeration of nanoparticles are insignificant at the micrometer scale. For this reason, simple mechanical shearing is often sufficient to disperse the cut fibers in almost any matrix, whereas long fibers are typically incorporated manually via meshes. Therefore, the glass surface treatments are used as a protective coating for the fiber, and to a lesser extent for improving the adhesion between the glass and the polymer, unlike with the nanoparticles, where surface treatments are mostly aimed at improving dispersion. Improving interfacial adhesion between glass fibers and a polymer matrix is a vital task when an efficient stress transfer from the polymer to the glass fiber is desired. Glass fibers have a significantly higher Young's modulus (~77 GPa)[7] compared to PC (~2.3 GPa)[31], which provides the composite material with superior mechanical properties than neat PC based materials. The weakest component in a composite is usually the interface; therefore, improving this interfacial

strength remains the focus of many studies. However a weak interface can also be beneficial in some cases, since it breaks and absorbs energy when a composite is subjected to stress, resulting in the toughening of the material[1]. It is now apparent that controlling the interface is more important than simply improving it.

The mechanical properties of many glass fiber/polymer systems have been well documented[1,2,10,33,34], and fiber sizings have been optimized to exploit these properties. Even though interfacial adhesion for glass fiber-polymer composites is understood to the point where they can quantify composite performance, a better understanding is still required in order to achieve control over the interface and optimize performance. It is therefore the goal of this chapter to relate the mechanical properties of composites to the interfacial work of adhesion (W_{adh}) and the interfacial shear stress (τ_{IFSS}), as measured and calculated in the previous chapter.

3.2 Experimental

Materials

The glass fibers were manufactured and silanized in the same manner as described in section 2.2. The main differences were that the fibers produced here were one 13 μm in diameter, and the silane and solvent volumes used were greater than in the process described earlier.

Composites Preparation

Initially, a twin screw extruder (Haake HBI System 90) was utilized to make PC composites with 10 wt% glass fibers; however, the silanizing procedure resulted in glass

fiber aggregates that resembled cotton balls. As a result, the fibers were expelled during the extrusion, excluding the fibers from the mixing process. To counter this, PC was melt pressed at 300 ^{O}C into 1mm thick sheets, and known amounts of fibers were sandwiched between the sheets. They were then melt pressed for a further 10 minutes; although this first step in processing yielded better dispersion of the glass fibers in the PC matrix, it also resulted in increased decomposition of PC. This resulted in sheets with uneven distribution of the fibers, which had to be pelletized and extruded at 275 ^{O}C using a micro-compounder, the Haake minilab, at Materials Research lab (MRL). The samples were extruded 3 grams at a time and recycled for 5 minutes. They were then dried overnight before being injection molded into flexure (ASTM D790) and tensile bars (ASTM D638-03) using an injection molder (BOY 22D). Commercial glass fibers were extruded (Haake HBI System 90) and injection molded without melt pressing because they were condensed enough to mix well with PC pellets. Random orientation of the fibers was noticed via optical microscopy for all samples.

Mechanical Testing

The composite tensile bars were tested using the tensile tester (Instron 5566) at a cross-head speed of 25 mm/min. The flexure tests were conducted with a strain rate of 2 mm/min.

UV-vis spectroscopy

UV-vis spectroscopy was done on the flexure bars in order to determine the yellowing index, and consequently, the degradation induced during processing.

3.3 Results and Discussion

Tensile and flexure tests were conducted on samples prepared with glass fibers silanized in the same manner as the pullout test. In addition, composites were also made with two commercial chopped fibers. The commercial fibers were designated as 415A-17C and 3790. The latter is designed to adhere greatly with PC, and therefore provides better mechanical properties. The composition of the coatings on these fibers is unknown; however, most commercial fiber coatings are known to have ~30 % silane coupling agents. The glass fiber concentration was maintained at 10 wt% in all cases. Tables 3.1 and 3.2 summarize the results obtained from the tensile test.

Table 3.1 Tesile strain and stress @ max tensile extension, tensile strength, and toughness for the composites tested. (10 wt% glass fibers)

Material	Tensile strain @ max. Tensile extension (%)	Tensile stress @ max. Tensile extension (MPa)	Tensile strength (MPa)	Toughness (MPa)
PC (Makrolon 3208)	100.9 ± 0.9	38.2 ± 1.1	64.9 ± 3.6	54.2 ± 0.4
415A -17C	34.7 ± 5.7	26.1 ± 2.0	60.0 ± 0.4	16.4 ± 2.7
3790	9.6 ± 0.8	50.1 ± 2.6	89.0 ± 3.2	5.5 ± 0.4
E-glass	43.2 ± 10.0	26.6 ± 0.2	63.9 ± 0.1	20.9 ± 5.1
CF_3 E-glass	31.0 ± 4.5	27.2 ± 0.2	62.6 ± 0.2	14.6 ± 2.2
CH_3 E-glass	29.2 ± 9.8	27.1 ± 1.2	64.7 ± 0.2	14.0 ± 5.0
NH_2 E-glass	16.8 ± 2.7	27.1 ± 0.9	61.8 ± 0.9	7.7 ± 1.3
OCH_3 E-glass	15.3 ± 2.0	26.1 ± 0.7	62.3 ± 0.4	7.1 ± 1.0

Table 3.2 Young's Modulus, Tensile strain and stress @ yield, tensile strength and elongation @ break for the composites tested. (10 wt% glass fibers)

Material	Young's modulus (MPa)	Tensile strain @ yield (%)	Tensile stress @ yield (MPa)	Tensile strength (MPa)	Elongation @ break(%)
PC (Makrolon 3208)	1458 ± 112	11.2 ± 1.6	60.2 ± 0.5	64.9 ± 3.6	100.9 ± 0.9
415A -17C	2043 ± 94	9.8 ± 0.9	60.0 ± 0.4	60.0 ± 0.4	34.7 ± 5.7
3790	2214 ± 87	9.5 ± 0.7	89.0 ± 3.2	89.0 ± 3.2	9.6 ± 0.8
E-glass	1884 ± 58	10.0 ± 0.4	63.9 ± 0.1	63.9 ± 0.1	43.2 ± 10.0
CF_3 E-glass	2070 ± 51	8.8 ± 0.5	62.6 ± 0.2	62.6 ± 0.2	31.0 ± 4.5
CH_3 E-glass	2046 ± 67	8.9 ± 0.7	64.7 ± 0.2	64.7 ± 0.2	29.2 ± 9.8
NH_2 E-glass	1832 ± 62	8.3 ± 0.9	61.8 ± 0.9	61.8 ± 0.9	16.8 ± 2.7
OCH_3 E-glass	1837 ± 39	7.9 ± 0.5	62.3 ± 0.4	62.3 ± 0.4	15.3 ± 2.0

Figure 3.1 compares representative engineering stress-strain curves for PC and the composites during the tensile tests. As expected, the 3790 composites displayed the highest tensile strength. The inset in the figure indicates that the modulus of the E-glass fiber composite compares well with the NH_2 composites, but the curve soon veers off towards the PC curve.

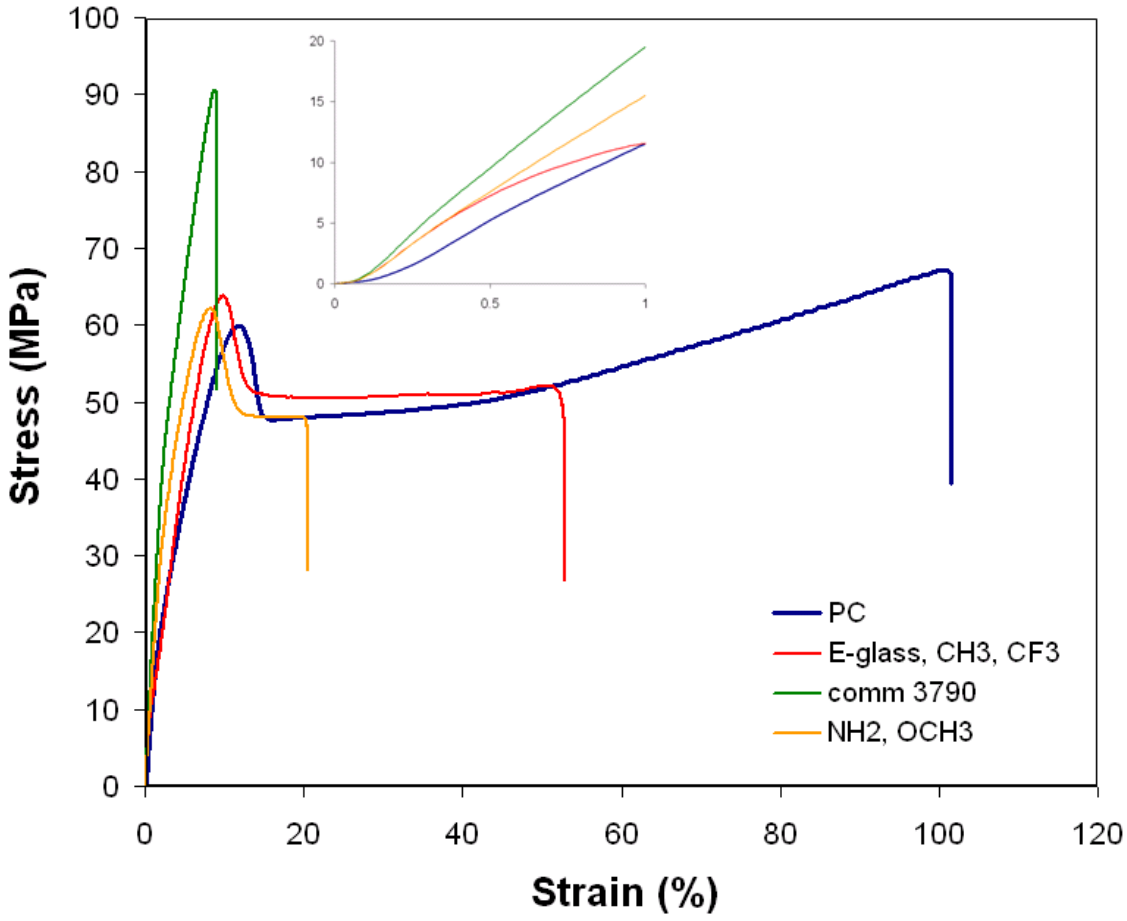

Figure 3.1 Schematic representation of engineering stress-strain behavior of the composites tested.

Composites made with 3790 fiber reported the highest tensile strength and Young's modulus, but have the lowest toughness, all indicative of a strong interface. This is not surprising since it was designed to have a strong interface with PC, however,

commercial fibers have protective coatings along with silane coupling agents which are known to improve interfacial adhesion. Hence, it is remarkable to see that fibers prepared in this study, and employing very simple SAM-only fiber treatments, compared fairly well with the commercial optimized 3790, despite their rather 'primitive' sizing compared to the commercial fibers.

3.3.1 Trends in Composite Toughness

The trend in the toughness of the different materials was consistent with standard composites' expectations. As noted in the introduction, a weak interface typically gives rise to a composite with a high toughness. Since commercial fiber 3790 is designed to have a strong interface with PC, it produced the lowest toughness value. NH_2 and OCH_3 composites also proved to have lower toughness, which was also expected since they were designed to achieve a strong interface. CF_3, CH_3, and 415A-17C samples gave toughness values that were indicative of a weaker interface. One exception that should be noted is that of E-glass, which reported the highest toughness of all composites. Based on work of adhesion calculations, E-glass composites should have given a toughness value intermediate between OCH_3, and CF_3. One possible explanation is that the presence of the silane inhibits interfacial crack propagation (rather diverts the crack back into PC) compared to the smooth interface between E-glass and PC. Since this debonding absorbs energy, a faster crack growth rate should result in improved toughness. One the other hand, the chemically inhomogeneous surface of silanized fibers may result in the yielding of the matrix rather than the interface.

Equally interesting was the toughness value for the NH_2 sample, which performed as expected. However, results from the pullout test suggested that NH_2 fibers have an intermediate adhesion to the interface. This discrepancy could be explained by the inhomogeneous surface energetics of the fiber resulting from cosilanization of ODMS and NHDMS on the fiber surface. During the pullout test, only a small part of the fiber is in contact with PC; as a result, local surface energy differences may play a role. In the case of composites however, the entire fiber is surrounded by the matrix, averaging out any such effects.

3.3.2 Comparisons of Composite Moduli

As shown in Table 3.3, similar trends are recorded for the Young's modulus and for the flexure modulus of the composites. The incorporation of reinforcements, regardless of interfacial adhesion, resulted in improvements in the moduli. Figure 3.3 correlates the Young's modulus to the τ_{IFSS} and W_{adh}.

Table 3.3 Young's modulus and flexure modulus comparison, and percent improvements in composites.

Material	Young's modulus (MPa)	% increase in modulus	Flexure Modulus	% increase in modulus
PC (Makrolon 3208)	1458 ± 112		2390 ± 63	
415A -17C	2043 ± 94	40	3169 ± 13	32
3790	2214 ± 87	52	3509 ± 204	47
E-glass	1884 ± 58	29	3251 ± 36	36
CF_3 E-glass	2070 ± 51	42	3425 ± 20	43
CH_3 E-glass	2046 ± 67	40	3371 ± 53	41
NH_2 E-glass	1832 ± 62	26	2829 ± 25	18
OCH_3 E-glass	1837 ± 39	26	2774 ± 47	16

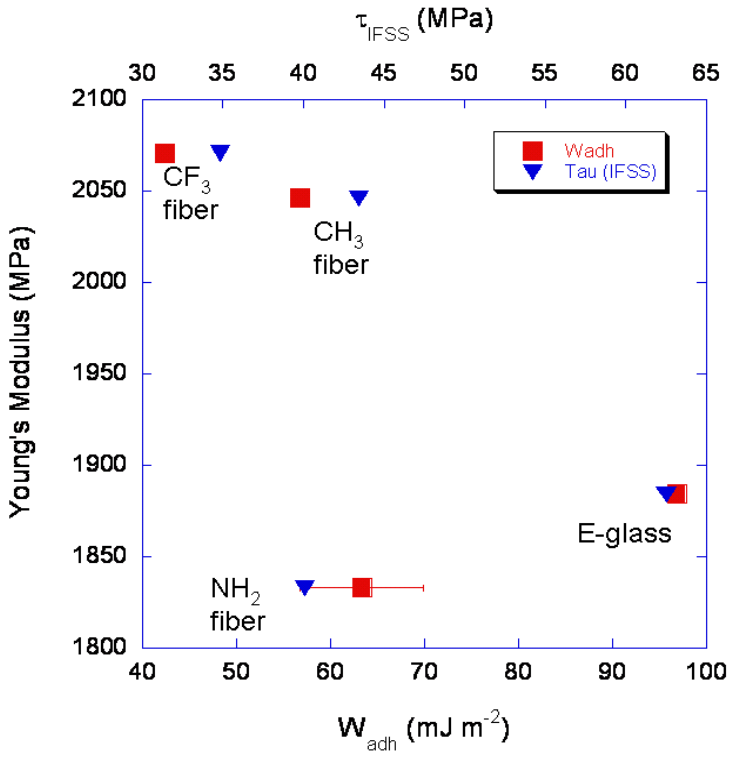

Figure 3.2 Correlation between Young's modulus and work of adhesion (square), and interfacial shear stress (triangle), for selected samples.

Surprisingly, the modulus seems to decrease as W_{adh} and τ_{IFSS} increase. Furthermore, NH_2 and OCH_3 samples had comparable modulus (~1830 MPa). These trends seem counterintuitive, especially since the former seem to adhere better with PC. For example, 3790 samples performed well due to increased interfacial adhesion, and the same was expected of the composites designed here. This anomaly most probably originated from polymer degradation, which was evident in the color of the composites, as shown in figure 3.3 and studied using UV-vis spectroscopy.

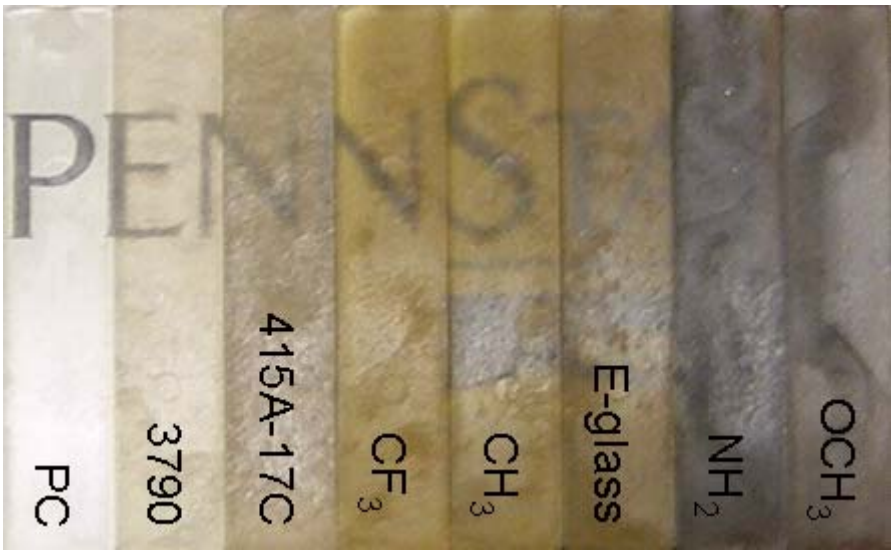

Figure 3.3 Flexure bars of composites made for this experiment. Progressive discoloration noticed for samples from left to right showing polymer degradation. Modulus tends to decrease is this order as well.

Composites made with the commercial fibers showed the least change in color, indicating minimal degradation. CF_3, CH_3, and E-glass samples degraded more, and NH_2 and OCH_3 seemed to have degraded even further. The degradation for each sample was studied using UV-vis spectroscopy, and the Friele's Yellowing Index (YI) (EQN 3.1) was calculated (ASTM E313).

$$YI = \frac{1}{2}\frac{(R+G)}{B} \qquad \text{(Equation 3.1)}$$

In Equation 3.1, R, G, and B, represent the transmittances of the red, green, and blue lights, respectively (wavelength = 680 nm, 530 nm, and 470 nm, respectively), obtained from the UV-vis spectrum. YI values for the samples shown in Figure 3.3 are graphed in Figure 3.4.

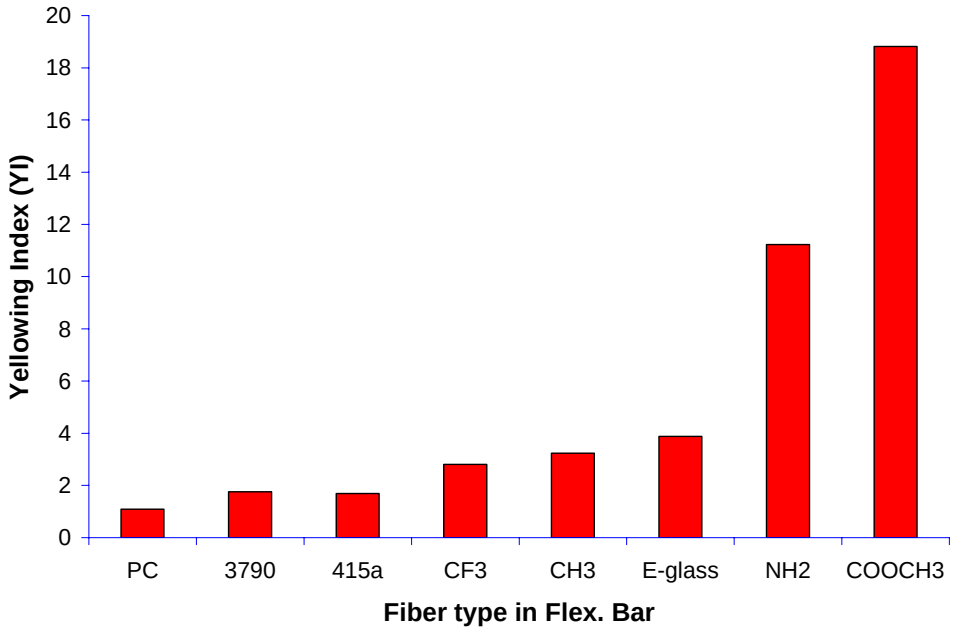

Figure 3.4 YI calculated from UV-vis spectra of samples shown in figure 3.3. Increase in YI follows the same trend as the discoloration.

As seen in the figure above, the YI increases in the same manner as the samples in Figure 3.3 show discoloration. FTIR/ATR was also conducted on thin films of samples prepared via solution casting. Comparisons of the FTIR/ATR spectra for the composites with that of PC did not reveal any new peaks. Also, the intensities of the existing peaks were different owing only to the difference in thickness of the samples. The spectra are given in Figure 3.5.

Fibers prepared in the lab, via the two-step process, resulted in the most degraded composites, probably because the polymer and fiber were exposed to elevated temperatures twice during sample extrusion/injection molding and during melt pressing. Samples made of commercial fibers were not subjected to this latter step. The additional degradation of OCH_3 fibers is thought to be the result of a trans-esterification reaction that occurs between the ester group of CDDMS and PC. Although the covalent bonds

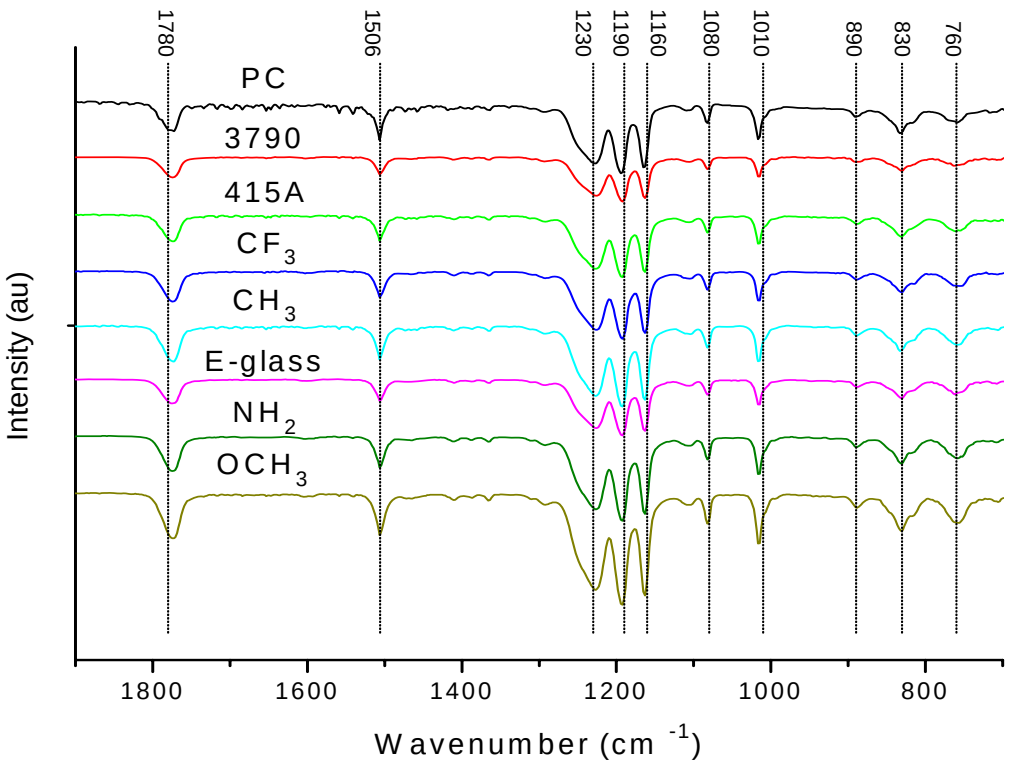

Figure 3.5 FTIR/ATR spectra for PC and the composites used for mechanical testing.

Table 3.4 Different peaks noticed in FTIR/ATR spectra of PC and composites. ψ means stretching.

Peak (cm^{-1})	Meaning
760	Aromatic C-H ψ [35]
830	Aromatic C-H ψ [35]
890	Aromatic C-H ψ [35]
1010	C-H ψ [36]
1080	O-H (phenol) ψ [37]
1160	ether bridge between aromatic rings ψ [35]
1190	assymetric SO_3^- ψ [38]
1230	C-N ψ [39]
1506	Aromatic C-C ψ [40]
1780	Carbonal group of PC ψ [41]

lead to increased interfacial strength, the effect is negated by the degradation of PC due to chain cleavage, resulting in a discolored composite. The decomposition of the PC for the

NH_2 fibers was expected, since PC is exceptionally sensitive to amine compounds. However, in this case there exist additives that can control PC thermal decomposition.

3.4 Summary

Composites of commercial fiber 3790 performed as expected, but it is remarkable that 'primitive coatings' fibers (silanized fibers without protective coatings) synthesized in house for this experiment performed comparably well with the commercial fibers that bear PC-optimized coatings. The toughness of a composite is a good indicator of the interfacial adhesion, such that a weak interface normally results in a tougher composite, was also correlated back to the previously measured τ_{IFSS} and W_{adh}. Despite having a high $\tau_{IFSS,}$ unsilanized E-glass fibers also showed the highest toughness of all composites tested here. Such behavior indicates that the silane and processing induced PC decomposition determined the mechanical properties of the composites. Also, an unexpected trend in the modulus of composites made of fibers silanized in this experiment is noticed. However, this can also be explained by the increased degradation, which indicates that in addition to glass fiber surface manipulations, composite properties are strongly dependant on the processing conditions.

Chapter 4 Conclusion

4.1 Conclusions

Contact angle measurements on glass slides that underwent the same treatments as the fibers gave results that were consistent with literature. Therefore, the assumption of having good silane coverage is justified. This also permits the use of surface free energies for different silanes obtained from literature.

The single fiber pullout test gave a fairly linear relationship between the thermodynamic work of adhesion (W_{adh}) and τ_{IFSS}, and therefore can be assumed to be a viable method to determine the interfacial adhesion between glass fibers and PC. The pullout tests revealed that, as expected, fibers silanized with TFCS resulted in a weaker interface, compared to the E-glass, which reported the highest τ_{IFSS} value of 62.5 MPa. Although the pullout tests for the OCH_3 samples gave no results, this actually indicates superior interfacial strength resulting from covalent bonding between CDDMS and PC. Also, the almost linear increase of τ_{IFSS} with the calculated W_{adh} allows for better control of interfacial strength for different applications.

Macromechanical tests results seemed to contradict the results obtained with the single fiber pullout tests. In particular, the high toughness value for E-glass composites and the low modulus of the OCH_3 composites were unanticipated. These anomalies are attributed to the minute surface roughness increase due to silanization, and also polymer degradation as a result of processing.

It is clearly observed that the interfacial study by the pullout test does not necessarily correspond directly to the macromechanical tests. This study reveals that although the interface plays an important role in the performance of composites, other factors such as processing also play a significant role and can diminish the influence of the interface.

4.2 Future Direction

The short-term future goals are derived from the findings in this study. In both the pullout test and macromechanical tests, glass fiber surface roughness is thought to give a better understanding of the nature of the pullout and influence the mechanical performance of the composites. Roughness analysis using Atomic Force Microscopy (AFM) has been used in the past, and is proposed to be used in this study as well. Surface characterization can also be done using Fourier Transform Infrared spectroscopy (FTIR) which would highlight the end functional groups of the silanes. Furthermore, polymer degradation should also be addressed, and Gel Permeation Chromatography (GPC) would be an ideal choice for this study.

The long term goals involve the inclusion in this study of the protective coatings that are applied to commercial fibers, and their influence on interfacial adhesion. This necessitates further pullout and mechanical tests.

Once a clear understanding of the silane coupling agents and protective coatings are acheieved, one of the future plans would include making glass fiber composites that are transparent, by the manipulation of the refractive index of the coatings and of the glass. All composites in this study produced hazy samples, and to overcome this hurdle would fulfill applications where high performance clear composites are required.

REFERENCE

1. Hoecker, F., Karger-Kocsis, J., J. *Appl. Poly. Sci.* 59, 139 **(1996)**
2. Mader, E., Grundke, K., Jacobasch, H. J., Wachinger, G., *Composites* 27, 739 **(1994)**
3. Mader, E., Jacobasch, H. J., Grundke, K., Gietzelt, T., *Composites: Part A* 27A, 907 **(1996)**
4. Feller, J. F., Grohens, Y., *Composites: Part A* 35, 1 **(2004)**
5. Jensen, R.E., McKnight, S.H., *Comp. Sci. and Tech*. 66, 509 **(2006)**
6. Brovko, O., Rosso, P., Friedrich, K., *J. Matr. Sci. Lett*. 21, 305 **(2002)**
7. Wallenberger, F. T., Watson. J. C., Li, H., *ASM handbook* 21
8. Chu, P. F., *Handbook of Polypropylene and Polypropylene Comp*. CRC press, **(2003)**
9. Piggot, M. R., Xiong, Y., *Fiber Matrix, and Inter. Prop*, STP 1290, 84 **(1996)**
10. Ramanathan, T., Schulz, E., Subramanian, K., *J. Reinforced Plastic. Comp*. 23, 1639 **(2004)**
11. Nam, G.J., Kim, H., Lee, J. W., *Poly. Comp*. 24, 487, **(2003)**
12. Ageorges, C., Friedrich , K., Ye, L., *Comp. Sci. Tech*. 59, 2101 **(1999)**
13. Feih, S., et al.*Testing Procedure for Single Fiber Fragmentation Test*, 87-550-3381-4 **(2004)**
14. Pitkethly, M. J., *Fiber Matrix, and Inter. Prop*, STP 1290, 34 **(1996)**
15. Weaver., J. H., et al., *J. Am. Ceram. Soc*. 89, 2869 **(2006)**
16. Zhang, B., Benmokrane, B., *J Matr. Civil Eng*. 14, 399 **(2002)**

17. Barber, A. H., Cohen, S. R., Kenig, S., Wagner, H. D., *Comp. Sci. and Tech*. 64, 2283 **(2004)**

18. Cooper, C. A., Cohen, S. R., Barber, A. H., Wagner, H. D., *Appl. Phys. Lett*. 81, 3873 **(2002)**

19. Barber, A. H., Cohen, S. R., Wagner, H. D., *Appl. Phys. Lett*. 82, 4140 **(2003).**

20. Van Oss, C., Chaudhury, M. K., Good, R. J., *Chem. Rev*. 88, 927 **(1988)**

21. http://polymer.bu.edu/Wasser/robert/work/node8.html

22. Israelachvili, J. N. *Intermolecular and Surface Forces*; Academic: New York, **(1985)**

23. Nuriel, S., Liu, L., Barber, A. H., Wagner, H. D., *Chem. Phys. Lett*. 404, 263 **(2005)**

24. Park, S., Jin, J., *J. Poly. Sci. Part B*. 41, 55 **(2003)**

25. Comyn, J., *Adhesion Science* Royal Society of Chemistry, **(1997)**

26. Fadeev, A. Y., McCarthy, T. J., *Langmuir* 16 7268 **(2000)**

27. Genzer, J., Efimenko, K., Fischer, D. A., *Langmuir* 18, 9307 **(2002)**

28. Khatri, O. P., Devaprakasam, D., Biswas, S. K., *Tribology Letters* 20, 235 **(2005)**

29. Onoe, H., Matsumoto, K., Shimoyama, I., J. *Microelec. Syst.* 13, 603 **(2004)**

30. Zhuang, Y.X., et al. J. *Micromech. Microeng*. 16 2259 **(2006)**

31. Makrolon 3208 PSD, Bayer Material Science.

32. Jiang, K. R., Penn, L. S., *Comp. Sci. Tech*. 45, 89 **(1992)**

33. Felix, A. H., Cardozo, N. S., Nachtigall, S. M., Mauler, R. S., *Macromol. Mater. Eng*. 291, 418 **(2006)**

34. Vipulanandan, C., Mebarkia, S., *J. Appl. Poly. Sci*. 50, 1159 **(1993)**

35. Ishimaru, K., et al. *J. Mater. Sci*. 42, 122 **(2007)**

36. Fan, Q., Pu, C., Smotkin, E. S., *Inst. Electrical and Electronics Engineers*. 1112 **(1996)**

37. Vorgelegt Von, Ph.D Thesis, University of Vienna **(2001)**

38. Hong, J. W., Kim, H. K., Yu, J. A., Kim, Y. B., *J. Appl. Poly. Sci*. 84, 132 **(2002)**

39. Sarac, A. S., Springer, J., *Surf. Coating Tech*. 160, 227 **(2002)**

40. Skourlis, T. P., McCullough, R. L., *J. Appl. Poly. Sci*. 52, 1241 **(1994)**

41. Huang, Z. H., Wang, L. H., *Makromol. Chem., Rapid Commun*. 7, 255 **(1986)**